JGR Oceans

RESEARCH ARTICLE
10.1029/2018JC014813

Wind-Based Estimations of Ocean Surface Currents From Massive Clusters of Drifters in the Gulf of Mexico

A. C. Haza[1], N. Paldor[2], T. M. Özgökmen[1], M. Curcic[1], S. S. Chen[1,3], and G. Jacobs[4]

[1]Rosenstiel School of Marine and Atmospheric Science, University of Miami, Miami, FL, USA, [2]The Hebrew University of Jerusalem, Jerusalem, Israel, [3]University of Washington, Seattle, WA, USA, [4]Naval Research Laboratory, Stennis Space Center, MS, USA

Key Points:
- The surface wind contributes significantly to the upper 60 cm transport in the Gulf of Mexico
- The transport in the upper 5 cm differs from the upper 60 cm, due to the wave contribution

Correspondence to:
A. C. Haza,
ahaza@rsmas.miami.edu

Citation:
Haza, A. C., Paldor, N., Ozgokmen, T. M. M., Curcic, M., Chen, S. S., & Jacobs, G. A. (2019). Wind-based estimations of ocean surface currents from massive clusters of drifters in the Gulf of Mexico. *Journal of Geophysical Research: Oceans*, *124*. https://doi.org/10.1029/2018JC014813

Received 28 NOV 2018
Accepted 3 JUL 2019
Accepted article online 9 JUL 2019

Abstract During the Lagrangian submesoscale experiment (LASER), 1,000 drifters were launched to sample the surface ocean flow in the northern Gulf of Mexico. Due to half a dozen strong winter storms, about 40% of the drifters lost their drogue. This unintended situation facilitated documentation of both near-surface (5 cm) and deeper (60 cm) flows. These depths are relevant to transport of oil spills, as well as marine debris, such as microplastics, a rapidly growing environmental problem. Here, we improve the surface Lagrangian current prediction by combining a state-of-the-art ocean forecast model with wind and wave data. The ocean surface velocities are obtained from the Navy Coordinate Ocean Model at 1-km horizontal resolution, while the wind and wave fields are from the Unified Wave INterface Coupled Model coupled atmosphere-wave-ocean model. Two Lagrangian parameterizations are tested: one is based on Ekman dynamics, and the other directly on the surface winds. LASER data set is then used to assess the performance of these formulations, as a function of wind/wave conditions, as well as geographic region. It is found that incorporation of wind and wave data into the ocean circulation model can lead to major prediction improvement, by reducing the average 2-day separation from the modeled and real LASER trajectories by a factor ranging from 1.4 to 4.9. This is a significant improvement for applications, where a rapid deployment of assets is needed, such as oil spill response, or other tracking problems.

1. Introduction

Among the many processes occurring in the aftermath of an oil spill is the scenario when the oil ends up floating at or near the surface. Depending on the different states it undergoes, the oil can emulsify under the wind action to occupy the upper meter and be entrained by this depth-integrated circulation (denoted here simply as "thick-oil"), or spread under calm conditions over top few cm of the surface (denoted as "thin-oil" here). The vertical flow can vary widely over the first few meters below the surface. It was measured recently using a combination of instruments that the current magnitude averaged over the upper 1 cm of the ocean was nearly 4 times the average over the upper 10 m, under mild conditions (winds less than 5 m/s; Laxague et al., 2018). Given such vertical shear in the upper ocean, measurements under a variety of wind and wave conditions are therefore paramount to predict the fate of oil spills, or for that matter, other marine debris, such as microplastics.

The Lagrangian submesoscale experiment (LASER) was an expedition carried out in the Gulf of Mexico (GoM) in the winter of 2016 with the purpose of measuring surface transport pathways in the northern GoM (NGoM), motivated by the 2010 Deepwater Horizon (DwH) event, the largest accidental marine oil spill in history (D'Asaro et al., 2018). LASER was based mostly on Lagrangian sampling, namely, deployment of 1,000 surface drifters, aimed at capturing both mesoscale nondivergent flows and submesoscale divergent flows without the spatial-temporal aliasing problems inherent in many other sampling techniques (Özgökmen & Fischer, 2012).

There were three large cluster releases of ecofriendly surface drifters (Figure 1a) each composed of a floater containing a GPS, and a drogue extending 60 cm below the surface (Novelli et al., 2017). Most of the launches occurred in the NGoM in the general vicinity of the DwH spill. One of the objectives of LASER was to document seasonal variability of surface flows, compared to the previous Grand Lagrangian Deployment (Poje et al., 2014) conducted in the summer of 2012. Strong storms occurred during most of the experiment due to the 2016 El Niño, resulting in about 40% of drogues detaching from the floater in the first 7 weeks

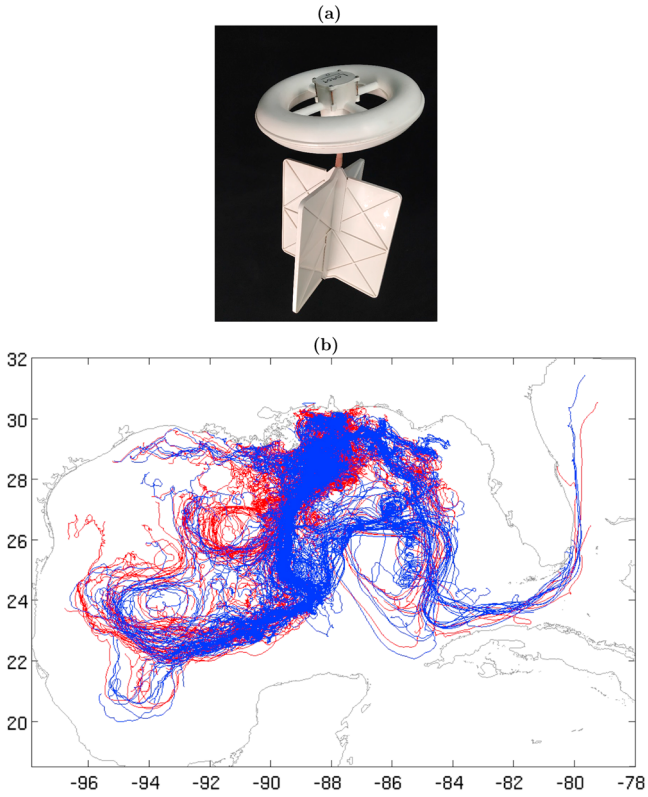

Figure 1. (a) The CARTHE drifter. (b) Lagrangian submesoscale experiment trajectories of the drogued (in blue) and undrogued (in red) drifters after 3 months of release in the Gulf of Mexico (longitude and latitude in the *x* and *y* axes, respectively).

(Haza et al., 2018). A consequence of this significant drogue loss is that the drifters ended up documenting two distinct types of flows: the upper 60-cm circulation from the drogued drifters (hereafter DD), with reduced surface wave impact (hence reduced Stokes drift), and the upper 5-cm flow from the undrogued drifters (or UD), which includes advection by the (much stronger) surface Stokes drift (Figure 1b). As discussed in Anis and Moum (1992), the ocean's mixed layer is not uniform but overlaid by a surface layer, the dynamics of which is governed by wave breaking, Langmuir cells, plume formation, shear due to wind stress, and Stokes drift. This layer is distinctly different from the underlying mixed layer, where convective eddies dominate. The existence of UD and DD incidentally provide valuable information on the gradient of the vertical shear very close to the ocean's surface. In the weeks following drogue losses, drifters sampled the NGoM and the GoM interior, often with overlapping DD and UD trajectories, allowing a documentation of such vertical shear over a large area, consisting of different dynamical regions and changing seas.

During LASER, the state-of-the-art data-assimilating ocean forecast model Navy Coastal Ocean Model (NCOM) was operated to guide drifter releases in the NGoM, where the circulation is known to be challenging. Near the coast, the surface currents on the continental shelf and slope are not estimated well by altimetric data assimilation. The existence of submesoscale flows near the experimental domain (D'Asaro et al., 2018; Poje et al., 2014) requires vastly more data than needed for mesoscales to use data assimilation in an effective way. Additionally, the strong vertical shear of the near-surface flows is not well captured by ocean models not only because it is not well resolved by the mesh spacings but also because of the enhanced air-sea interaction from many frontal passages and gust events associated with the strong 2016 El Niño.

We have implemented wind-based Lagrangian parameterizations using existing forecast fields from NCOM and the extensive LASER drifter data set in order to

(i) use this unique data set to infer the role played by the wind in the very near surface transport;
(ii) assess model performance; and
(iii) improve prediction of surface passive tracers.

The addition of a wind-based component to the near-surface particle advection in conjunction with an ocean current product is not a new approach in either the oil spill response community or in general physical oceanography. It was initially estimated by Kenyon (1969) that the surface Stokes drift for fully developed seas ranges between 1.6% and 3.6% wind speed measured at a height of 19.5 m. Addition of 3% wind to circulation model velocities, to account for direct wind shear on surface transport, is a standard approach in oil spill modeling (Le Hénaff et al., 2012). Lagerloef et al. (1999) reconstructed tropical surface currents by combining satellite altimetry with wind stress using a physically based statistical model, calibrated using 15-m drogued surface velocity Program (SVP) drifters. The steady-state model assumed a uniform slab of water, over which the observed wind stress is uniformly distributed. Time dependence was added by Paldor et al. (2004), who developed a hybrid Lagrangian-Eulerian model to estimate trajectories of near-surface drifters using data collected in the Pacific Ocean. The oceanic application of this hybrid Lagrangian-Eulerian model followed successful applications of the same model in the interpretation of field campaigns in the stratosphere (Dvorkin et al., 2001) and the troposphere (Paldor et al., 2002). More recently, Stanichny et al. (2016) estimated surface wind-driven currents in the Black Sea by combining wind, drifters, and altimetry. SVP-derived velocities were parameterized as a function of the wind amplitude coefficient and the rotation angle between wind and residual current direction at 15-m depth.

The question still remains on how to combine wind products with ocean models, in an era when the ocean circulation models with progressively increasing resolution capture finer-scale processes near the ocean's surface as well as horizontally. In other words, it is unclear whether there is a need to incorporate wind forcing in addition to the surface currents simulated by state-of-the-art ocean models. If so, what would be the optimal combination of modeled currents and winds?

The work presented here differs from others mainly in that the number of drifters in the LASER data set is unprecedented. In comparison to studies based on just several sets of drifters, statistics from 1,000 drifters is helpful to increase the validity of the results. The data set also consists of drifters following currents at two shallow depths, namely, 0.05 and 0.60 m versus 15 m, compared to far more sparse data sets used thus far. We use also NCOM as the surface ocean velocity field, which was operated in real time during the LASER at high resolution. The satellite altimetry is incorporated in the model via data assimilation (Jacobs et al., 2014). The altimetry is reliable to a certain degree in the GoM interior. However, the LASER data set covers a relatively short period of about 2.5 months and high temporal resolution exceeding that of the altimetry AVISO product. Away from the coastline, the surface flow in the NGoM is less constrained than the interior by geostrophy, leaving the surface winds as the most likely forcing factor influencing transport of material near the surface of the ocean. Furthermore, the wind-based parameterizations benefit from the high-resolution wind and wave forecasts supplied by the Unified Wave INterface Coupled Model (UWIN-CM), which was operating in real time as well during LASER.

We test two different types of Lagrangian wind parameterizations: the first is the same one developed by Paldor et al. (2004). It is based on Ekman dynamics within a slab of water of thickness H. The change of setting from a 15-m depth-integrated transport (comparison to SVP) to upper 60- and 5-cm flows is expected to translate into significantly different parameter ranges for optimal performance. The other parameterization is much simpler and consists of adding a fraction (typically a few percent, as stated above) of the 10-m wind velocity directly to the ocean model velocities. Seeing that we are dealing with higher wind frequencies and near-surface flows, a direct wind momentum injection may not differ too much from the Ekman solution but consists of a much simpler implementation. This simple model is often used to account for the effect of waves on surface oil transport. As such, it is of interest to evaluate the validity of the 3% rule using the extensive LASER data set. The validation from the CARTHE drifter data allows us to approximate the wind contribution for the two types of oil, that is, thick (emulsified and dispersed by wind) and thin surface (calm wind conditions) oils. We also differentiate between calm-to-moderate winds and strong winds. And finally, we analyze separately the NGoM and interior of the Gulf, since the geostrophic velocities away from the shelf and slope are more likely to be accurate by data assimilation. The wind and wave contribution to surface flows under strong mesoscale coherent structures is another problem on which we will try to shed some insight as well. Overall, the wind-based ocean surface currents are investigated for a total of $2^3 = 8$ different scenarios, summarized in Table 1.

Table 1
The Eight Different Scenarios Explored in This Study From the Results of the LASER Drifter Data Set

Domain	Oil/drifter type	Wind strength
NGoM	Thick/DD	High
NGoM	Thin/UD	High
NGoM	Thick/DD	Low
NGoM	Thin/UD	Low
Interior	Thick/DD	High
Interior	Thin/UD	High
Interior	Thick/DD	Low
Interior	Thin/UD	Low

Note. These are based on the geographical domain (NGoM or GoM interior), oil thickness ("thick-oil" for DD or "thin-oil" for UD), and wind strength (high or low) and constitute the *experimental matrix*. LASER = Lagrangian submesoscale experiment; GoM = Gulf of Mexico; NGoM = northern GoM; DD = drogued drifters; UD = undrogued drifters.

The paper is organized as follows: the Lagrangian parameterizations are described in section 2. The ocean and wind models are introduced in section 3. The results are presented in section 4. We conclude in section 5.

2. The Lagrangian Parameterizations

2.1. The Wind Stress Parameterization

This Lagrangian parameterization (Paldor et al., 2004) modifies the model velocity $\mathbf{V}_{\text{mod}}$ by adding a "correctional velocity" $\mathbf{V}_{\text{cor}}$ based on wind-stress considerations, such that the linear combination of both velocities becomes closer to or equal to the near-surface, 2-D horizontal drifter velocity $\mathbf{V}_{\text{dr}}$ sampling the flow of interest, as follows:

$$\mathbf{V}_{\text{dr}} = \alpha \mathbf{V}_{\text{cor}} + (1-\alpha)\mathbf{V}_{\text{mod}} \quad , \tag{1}$$

where $0 \leq \alpha \leq 1$ is the fraction of drifter velocity deviating from the ocean model velocity. $\mathbf{V}_{\text{cor}}$ is calculated by using a slab model. It is assumed that the drifter is drogued over a vertical span of H. The momentum equations are vertically averaged over a depth of H. In spherical coordinates, the components of the momentum equation in 2-D become

$$\begin{cases} \frac{\mathrm{d}u_{\text{cor}}}{\mathrm{d}t} = v_{\text{cor}} \sin(\theta)\left[2\Omega + \frac{u_{\text{cor}}}{R\cos(\theta)}\right] + \frac{\Gamma^x}{H} - \gamma u_{\text{cor}} \\ \frac{\mathrm{d}v_{\text{cor}}}{\mathrm{d}t} = -u_{\text{cor}} \sin(\theta)\left[2\Omega + \frac{u_{\text{cor}}}{R\cos(\theta)}\right] + \frac{\Gamma^y}{H} - \gamma v_{\text{cor}} \end{cases} , \tag{2}$$

where R is the Earth's radius, Ω the Earth's rotation frequency, θ is the latitude, $\Gamma^{x,y}$ are the zonal and meridional components of the wind stress divided by the water density, and γ is the Rayleigh friction coefficient.

Equation (2) is then nondimensionalized, scaling time by $1/(2\Omega)$ and length by R (velocity scale becomes $2\Omega R$). The nondimensionalized version of equation (2) becomes

$$\begin{cases} \frac{\mathrm{d}u^*_{\text{cor}}}{\mathrm{d}t^*} = v^*_{\text{cor}} \sin(\theta)\left[1 + \frac{u^*_{\text{cor}}}{\cos(\theta)}\right] + \frac{\tau^x}{\delta} - \gamma^* u^*_{\text{cor}} \\ \frac{\mathrm{d}v^*_{\text{cor}}}{\mathrm{d}t^*} = -u^*_{\text{cor}} \sin(\theta)\left[1 + \frac{u^*_{\text{cor}}}{\cos(\theta)}\right] + \frac{\tau^y}{\delta} - \gamma^* v^*_{\text{cor}} \end{cases} , \tag{3}$$

with $\tau^{x,y} = \Gamma^{x,y}/(2\Omega R)^2$, and $\delta = H/R$.

Once the velocity correction is calculated, the drifter position is obtained by integrating the combined modeled and wind-stress-corrected velocities along the longitudinal and latitudinal directions:

$$\begin{cases} \frac{\mathrm{d}\lambda}{\mathrm{d}t} = \frac{1}{\cos(\theta)} \quad u^*_{\text{dr}} = \frac{1}{\cos(\theta)}\left[\alpha u^*_{\text{cor}} + (1-\alpha)\, u^*_{\text{mod}}\right] \\ \frac{\mathrm{d}\theta}{\mathrm{d}t} = v^*_{\text{dr}} = \alpha v^*_{\text{cor}} + (1-\alpha)\, v^*_{\text{mod}} \end{cases} . \tag{4}$$

The ocean and wind-stress frequencies are $(3\ \mathrm{hr})^{-1}$ and $(1\ \mathrm{hr})^{-1}$, respectively. An advection time step of 15 min is chosen to limit numerical errors from time integration, and to match the 15-min time interval of the quality-controlled LASER drifter positions. A third-order polynomial routine is used for spatial interpolation.

2.2. The Wind and Wave Parameterization

For the direct wind parameterization, it is assumed that the added wind-based velocities are a fraction of the standard 10-m winds without any Coriolis deviation. The implementation of the Stokes drift in the GoM can also be simplified by the absence of remote swells, which was confirmed in Haza et al. (2018). Thus, the surface Stokes drift for this particular application can be considered a direct byproduct of the wind vector, particularly in highly variable winds when the anti-Stokes component does not have time to develop (Polton et al., 2005).

$\mathbf{V}_{\mathrm{dr}}$ in this parameterization is a linear combination of modeled ocean currents and the 10-m wind (or Stokes drift) contribution for $\mathbf{V}_W$:

$$\mathbf{V}_{\mathrm{dr}} = a \quad \mathbf{V}_{\mathrm{mod}} + b \quad \mathbf{V}_W \quad , \tag{5}$$

where $\mathbf{V}_W$ is either the surface wind field $\mathbf{V}_{10}$, or the surface Stokes drift $\mathbf{V}_{\mathrm{St}}$ from the UWIN-CM model, and the parameter b is a number between 0 and 1. For the wind case, we picked $0.01 \leq b \leq 0.05$, corresponding to only a few percent of the wind speed. We also experiment with wave parameterization, denoting it Stokes drift parameterization, where the parameter is taken as $b = 1$, since the full vector is included. Note, however, that the objective here is to verify that the assumptions made about the Stokes drift in the GoM are indeed correct, by testing the wind-wave alignment this time from the optimization of the parameterization's performance.

The range for the modeling contribution parameter is $0 \leq a \leq 1$. In order to compare to the wind-stress parameterization, we also add the option of not including the model velocity in the drifter advection.

3. Methodology

3.1. Data: LASER Surface Drifters

The LASER surface drifter (Figure 1a) is relatively cheap, composed of a mostly biodegradable floater and sail, and designed to minimize wave rectification and wind slip, in order to accurately track the average horizontal current in the upper 60 cm. The GPS units are set to transmit their position every 5 min with an accuracy of 5–7 m and can last up to 3 months. However, the quality-controlled trajectories are sampled at a 15-min interval (Haza et al., 2018).

LASER is in part composed of three large drifter deployments consisting of 300 each, with different objectives: The Phase 1 (P1) deployment aimed to reenact part of the Grand Lagrangian Deployment of summer 2012 (Berta et al., 2015; Curcic et al., 2016; Olascoaga et al., 2013; Poje et al., 2014) under wintertime conditions, when submesoscale features are more active (Mensa et al., 2013). A rapidly deployed cloverleaf pattern, consisting of nodes with drifter triplets and spanning an area about 7 km × 7 km, was employed for P1 to measure multiscale dispersion with roughly 300 drifters. The Phase 2 (P2) deployment was aimed to follow the evolution of a surface front on the edge of a Mississippi River plume. This front was adaptively reseeded as drifters dispersed along the convergence zone. . Finally, the Last Drifter Array (LDA), which was part of Phase 4 (P4), was focused on the evolution of a submesoscale dipole using a rectangular array with 1-km spacing spanning an area about 16 km × 19 km (Figure 1). To optimize the placement of each deployment, survey lines of drifters were also released.

Strong storms occurred during LASER as the result of the 2016 El Niño, with the most intense episodes occurring on 22 and 27 January, 5, 9, 15, and 24 February, and 9 March. The recurring high-wind speed deviations from climatological statistics can be seen in Figure 4f of Judt et al. (2016). In particular, major storms occurred 1–2 days after the P1 (21 January) and the LDA (7 February) launches. A significant fraction of the drifters lost their drogues. It was found that the UD had a very distinct behavior based on their response to the wind and GPS transmission anomalies. Thanks to the persisting high drifter density, it was possible to rely on averaged local spatial velocity differences to estimate iteratively the drogue loss times with high accuracy (Haza et al., 2018). Thus, the 40% drogue losses effectively split the data set into two categories: the DD sampling the depth-integrated 60 cm without the net effect of the surface waves, and the UD sampling the upper 5 cm, including the Stokes drift and other by-products of the ocean-atmosphere interface.

Table 2
Summary of the Forecast Models Main Components

Output fields	NCOM	UWIN-CM
Ocean:	**Ocean**	Ocean, **Wind**, **Waves**
	NCOM	HYCOM v2.2
	OTIS tidal	tidal
	0.01° res.	0.04° res.
	data assimilation	no data assimilation
Winds:	COAMPS	**WRF**
	0.2° res.	**4 km res.**
Waves:	n/a	**UMWM**

Note. Those used in this study are highlighted in bold font. NCOM = Navy Coordinate Ocean Model; UWIN-CM = Unified Wave INterface Coupled Model; WRF = Weather Research and Forecasting; OTIS = Ocean Tide Inverse Solution; UMWM = University of Miami Wave Model; COAMPS = Coupled Ocean/Atmosphere Mesoscale Prediction System.

When DD and UD overlap, the LASER data set provides estimates of the vertical shear near the surface, which is an additional source of information. About 10,600 instances were found in the NGOM when DD and UD intersected within $0.05° \times 0.05°$ ($\sim 5.5 \times 5.5$ km^2) bins at 15-min intervals. We thus define DV as the bin-averaged Lagrangian velocity difference $V_{UD} - V_{DD}$ at a given time.

3.2. Ocean Atmosphere and Wave Modeling

Two operational models were used during LASER: one producing ocean forecast fields at high resolution (the Navy Coordinate Ocean Model), with realistic tidal and river forcings, and the other producing high-resolution forecast wind and wave fields (UWIN-CM).

For the implementation of the Lagrangian parameterization, we relied on NCOM for the ocean model, which is submesoscale permitting and has data assimilation, and on UWIN-CM for the surface winds and Stokes drift. See Table 2 for a summary of the model components used in this study.

3.2.1. The Ocean Circulation Product (NCOM)

The NCOM forecasts were conducted in real time during the LASER. The high horizontal resolution (1 km) is intended to explicitly resolve part of the submesoscale spectrum. The model experiment is forced by the atmospheric conditions from the Coupled Ocean/Atmosphere Mesoscale Prediction System (COAMPS) system (Hodur, 1997). Data assimilation of available satellite and in situ observations is conducted (Jacobs et al., 2014). The mesoscale coherent structures are realistically located in NCOM due to the altimeter assimilation. The surface wind stress is determined from the atmospheric model wind velocity. Surface heat fluxes are computed using bulk flux formulations that use the 10-m air-temperature and humidity along with the ocean model SST. Tidal potential forcing is applied to the inner domain, and tidal boundary conditions for water level and barotropic velocity are provided by the Oregon State University global Ocean Tide Inverse Solution (Egbert & Erofeeva, 2002). Thus, locally generated tides are present in the model.

During LASER, the NCOM forecast fared reasonably well in the GoM interior because it can constrain to a certain degree the mesoscale field via assimilation of altimetry-based Sea Surface Height. However, the lack of oceanic constraints in the NGoM away from the coast and river outflows was challenging for ocean prediction. This is confirmed in the optimal results of the wind-based parameterizations of section 4.2. Two fairly good representatives of the ocean model skill during this experiment are displayed in Figure 2: a pseudo-Eulerian map was generated by computing a daily velocity average in $0.1° \times 0.1°$ bins for a given day. An example of generally good agreement with observations is illustrated in Figures 2c and 2d, where the LASER drifters were entrained in the GoM interior by a strong mesoscale feature called the Tiger-Tail around 5 February. NCOM successfully captured the general direction of the flow in this region, albeit with slightly weaker momentum. Note that satellite altimeters do not provide sufficient spatiotemporal coverage

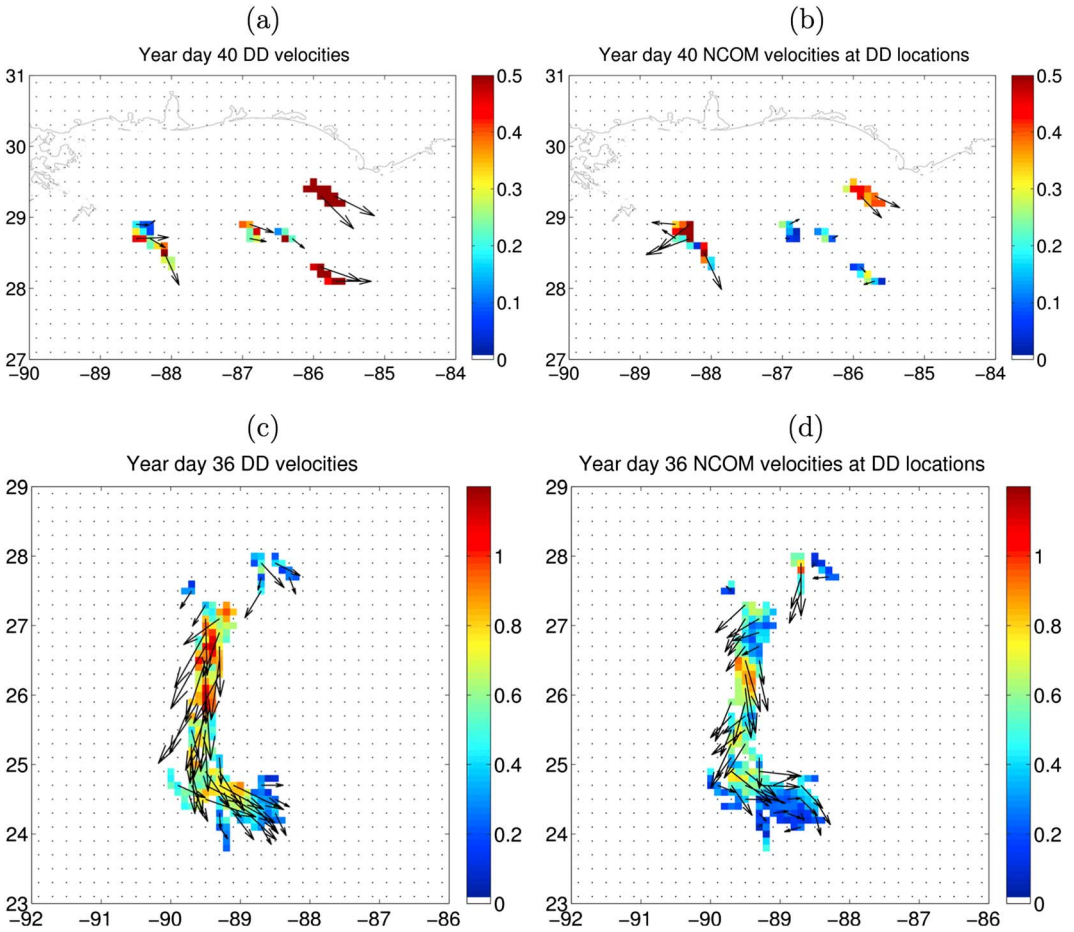

Figure 2. (a) Pseudo-Eulerian representation of the flow field from the drogued LASER drifter velocities on yearday 40 in the northern Gulf of Mexico. (b) Corresponding NCOM velocities from the same trajectory locations. (c) Same as (a) in the Gulf of Mexico interior on yearday 36. (d) Corresponding NCOM velocities from the LASER drifter trajectories of (c). Color units are meters per second. NCOM = Navy Coordinate Ocean Model; LASER = Lagrangian submesoscale experiment; DD = drogued drifters.

to capture the full velocity spectrum of the mesoscale field. On the other hand, the forecasted velocities of 9 February in the NGoM differ substantially where drifters are present (Figures 2a and 2b).

3.2.2. The Wind and Wave Products (UWIN-CM)

We use highly realistic winds and waves from a coupled ocean-atmosphere-wave model to implement the parameterization for $\mathbf{V}_{\mathrm{cor}}$ and $\mathbf{V}_{W}$. The source for the synoptic wind and wave data used in this study is the UWIN-CM (Chen & Curcic, 2016; Chen et al., 2013). It is designed as a multimodel system with the flexibility of exchanging individual model components for the atmosphere, waves, ocean, land, and sea ice. The model has been used to study the role of Stokes drift in surface transport (Curcic et al., 2016), the impacts of coupling on boundary layer structure (Zhu et al., 2016) and storm surge prediction (Dietrich et al., 2018) in Hurricane Isaac in 2012, and the influence of atmospheric forcing on the transport in the GoM on diurnal and seasonal scales (Judt et al., 2016). Here, the system consists of fully coupled atmosphere, surface wave, and ocean circulation models.

The atmosphere model used within UWIN-CM is the nonhydrostatic Weather Research and Forecasting (WRF) model v3.7.1 with the Advanced Research WRF dynamical core (Skamarock et al., 2008). WRF is configured with 36 vertical layers and a 12-km horizontal resolution on the domain (103°W to 55°W, 7°N to 45°N), with a 4-km resolution nest covering the entire GoM.

The surface wave model used within UWIN-CM is the spectral University of Miami Wave Model version 2 (Donelan et al., 2012). It is configured with 4-km grid spacing for the inner nested domain. The wave energy

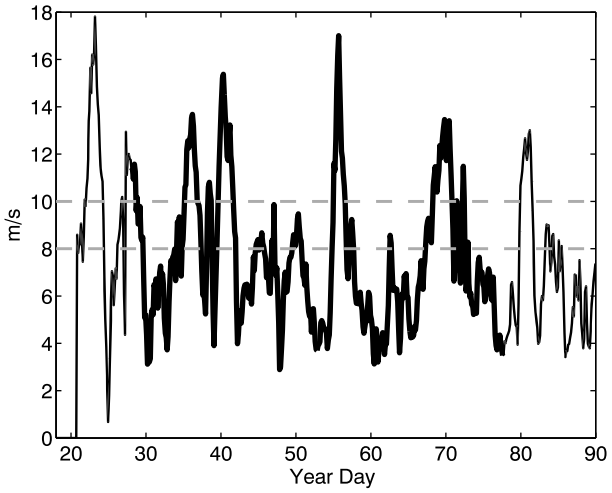

Figure 3. Time series of the Unified Wave INterface Coupled Model 10-m winds averaged over the Lagrangian submesoscale experiment drifter array. The dashed lines mark the limits for "low winds" and "high winds."

spectrum is represented by 36 directional bins and 37 frequency bins that range from 0.0313 to 2 Hz on a logarithmic scale.

The three-dimensional Stokes drift fields (Phillips, 1977; Stokes, 1847) for this study are evaluated by computing the full integral over the wavenumber directional space:

$$\mathbf{u}_{\mathrm{St}} = \int_0^{2\pi}\int_0^{\infty} \omega k^2 \frac{\cosh[2k(\mathrm{d}+z)]}{2\sinh^2 kd} F(k,\theta)\,\mathrm{d}k\,\mathrm{d}\theta, \tag{6}$$

where ω is the angular frequency, k is the wavenumber, d is the mean water depth, z is the distance from the surface (negative-downward) at which the Stokes drift field is being evaluated, F is the wavenumber energy spectrum, and θ is the direction of the waves.

Finally, the ocean circulation model used within UWIN-CM is the HYbrid Coordinate Ocean Model (HYCOM) version 2.2 (Wallcraft et al., 2009) with full tidal forcing. It is a three-dimensional hydrostatic ocean model with hybrid vertical coordinates: z levels in shallow water, terrain-following coordinates in intermediate water, and isopycnal (constant density) coordinates in deep water. HYCOM is configured with 0.04° (roughly 4 km) horizontal grid spacing and 32 vertical levels on the WRF outer domain.

The coupling between atmosphere-ocean-wave models is implemented using the Earth System Modeling Framework (Hill et al., 2004). Fields between all components are exchanged every 60 s. Initial and lateral boundary conditions were taken from the National Center for Environmental Prediction Global Forecasting System daily forecasts at 0.25° horizontal resolution for WRF and from the global, data assimilating, 0.08° horizontal resolution daily HYCOM fields for the ocean model.

For LASER, daily 72-hr forecasts were generated from 1 January to 1 April 2016. Each daily forecast is initialized from Global Forecasting System and global HYCOM fields for the atmosphere and ocean components, respectively. The wave model is initialized from the previous day's forecast. To obtain continuous fields of surface wind and Stokes drift during the LASER drifter analysis period, the 24- to 48-hr periods of each forecast were concatenated.

The wind stress in UWIN-CM is obtained after calculating both the skin drag and the form drag from the wave field, at an hourly rate.

3.3. Experimental Setting

The implementation of the parameterizations goes through eight scenarios (Table 1) based on the location, wind intensity, and oil thickness, defined as follows:

(a) Location: We consider two domains, separated by the latitude 28°N. Within the context of LASER, north of 28°N encompasses the continental shelf and slope, or NGoM, where mesoscale presence is weak. South of this latitude the drifter trajectories mainly occupy the open ocean of the GoM, or GoM interior, where the mesoscale flows and the Loop current system are dominant.
(b) Wind events: high wind versus low wind events. These events last about 1–3 days. There were eight high wind events and six low wind events during LASER, where *low* is defined as $U_{10} < 8$ m/s winds and *high* as $U_{10} > 10$ m/s winds (see Figure 3 and Table 3).
(c) Oil thickness: The two thickness values correspond to the 60-cm drogued (or thick layer oil) versus 5-cm undrogued (or thin layer oil) CARTHE drifters.

The parameterizations are applied to an ensemble of trajectories within a given wind event. The initial conditions correspond to a subset of the LASER drifter positions at the beginning of the event. The advection period does not exceed 2 days, which is the forecasting period and the most relevant time for recovery applications.

The performance of the parameterization is evaluated by comparing the 2-day trajectories to those of the LASER data set with same initial conditions as follows: D_i is the mean 2-day separation (from t_0 to t_0+48hr)

Table 3
High and Low Wind Events During the LASER

Wind event	Type	Start (yearday)	End (yearday)
1	high	22.1979	23.7604
3	high	27.2083	28.4479
5	high	35.2188	36.2604
6	high	39.5938	41.4688
8	high	55.0104	56.0521
11	high	69.0729	71.1562
12	high	71.9896	72.4062
14	high	79.8021	81.5729
2	low	24.2812	26.3646
4	low	29.4896	34.1771
7	low	50.8438	54.4896
9	low	57.6146	61.7812
10	low	64.9062	66.9896
13	low	76.3646	79.4896

Note. Start and end dates of each event are given in year day of 2016. LASER = Lagrangian submesoscale experiment.

between a calculated trajectory of index i and the corresponding observed trajectory of LASER drifter i:

$$D_i = \frac{1}{48 \quad \text{hr}} \int_{t_0}^{t_0+48 \quad \text{hr}} ||\mathbf{X}_i^c(t) - \mathbf{X}_i^{\text{obs}}(t)|| \quad \text{d}t \quad , \tag{7}$$

where $\mathbf{X}_i^c(t)$ and $\mathbf{X}_i^{\text{obs}}(t)$ are the calculated and observed position vectors of drifter i at time t, respectively. The improvement factor IF is then defined as

$$IF = \frac{\sum_{i=1}^{i=N} D_i(\text{model})}{\sum_{i=1}^{i=N} D_i(\text{param})} \quad , \tag{8}$$

where the summation refers to the ensemble of N trajectories. Thus, $IF = 1$ means no improvement, while $IF < 1$ means that the parameterization yielded predicted trajectories that were farther away from the observed trajectories compared to the trajectories generated by the model with no parameterization. An improvement is seen for $IF > 1$, and it can be quantified as a percentage corresponding to $(IF - 1) * 100$.

The hybrid (wind-stress based) parameterization described by equations (3) and (4) has three parameters: δ, γ^*, and α. The improvement factor is usually interpolated in two dimensions as a function of (α, γ^*) for a fixed ratio δ. α covers the entire range of possible values, from NCOM only ($\alpha = 0$, leading to IF=1) advection, to V_{cor} only ($\alpha = 1$) advection. As explained in Paldor et al. (2004), $1/\gamma^*$ corresponds to a velocity relaxation time. Therefore, if $1/\gamma^* = N$ days, then the nondimensional Raleigh coefficient $\gamma^* = (4\pi N)^{-1} = 0.08/N$. We picked 1 hr for the smallest relaxation time, that is, the time resolution of wind outputs from UWIN-CM, which corresponds to the highest γ^* value of 1.9. Thus, $0.1 \leq \gamma^* \leq 1.9$.

The wind parameterization has only two parameters (equation (5)): The IF is also function of (a, b) with $0 \leq a \leq 1$ and the wind percentage $0\% \leq b \leq 5\%$. For $a = 1$ and $b = 0$, $IF = 1$.

The optimal parameter sets (for both parameterizations) are also compared to the wind and wave contributions estimated in the LASER vertical shear ΔV.

4. Results

Due to the different types of results presented in this section, the layout and variables involved or compared are displayed in Table 4 for clarity.

Table 4
Structure of Section 4 With a List of Comparisons

Results	Variables comparison	Section
LASER vertical shear		4.1
	Stokes v.s. wind (UWIN-CM)	4.1
	DV (LASER) versus Stokes, wind (UWIN-CM)	4.1
	DV (LASER) versus lab experiments	4.1
Experimental matrix		4.2
	thick versus thin-oil, high winds	4.2.2
	thick v.s. thin-oil, low winds	4.2.2
	thick-oil, high versus low winds	4.2.2
	thin-oil, high versus low winds	4.2.2
	NGoM versus Interior	4.2.3
	Stokes versus wind	4.2.4
	without ocean model	4.2.5
	this work versus past studies	4.2.6
Individual events		4.3
	Clover, high wind Event 1	4.3
	LDA, high wind Event 6	4.3

Note. LASER = Lagrangian submesoscale experiment; UWIN-CM = Unified Wave INterface Coupled Model; LDA = Last Drifter Array; NGoM = northern Gulf of Mexico.

4.1. LASER Vertical Shear and Stokes Drift

As the LASER drifter (DD) was designed to minimize the effect of the surface waves (Novelli et al., 2017), it is expected that the velocity differential of the DD and UD overlaps. *DV* includes the surface Stokes drift as felt by the untethered floater, and a wind slip component due to the additional emerged part of the UD. Both components are estimated by comparing *DV* to the Stokes drift and 10-m winds of UWIN-CM (see Table 5).

The following cases are highlighted:

Table 5
Summary of DV's Dependence (as Illustrated in Figure 4) on the UWIN-CM Surface Stokes Drift and 10-m Winds for Several Values and/or Ranges of the Wind Magnitude

V_{wind} (m/s)	V_{Stokes} (cm/s)	$\langle DV_{proj}/V_{Stokes}\rangle$
> 14	> 20	1.08
[8–14]	[10–20]	1.29
[5–8]	[5–10]	2.11
V_{wind} (m/s)	V_{Stokes} (cm/s)	$V_{Stokes}(V_{wind}$ %)
15.5	25	1.61
14	20	1.51
11.5	15	1.36
8	10	1.2
5	5	0.86
V_{wind} (m/s)	V_{Stokes} (cm/s)	*DV* (% wind)
> 14	> 20	1.65
[8–14]	[10–20]	1.7

Note. The surface Stokes drift is also expressed as a fraction of the 10-m wind speed (also from UWIN-CM). UWIN-CM = Unified Wave INterface Coupled Model.

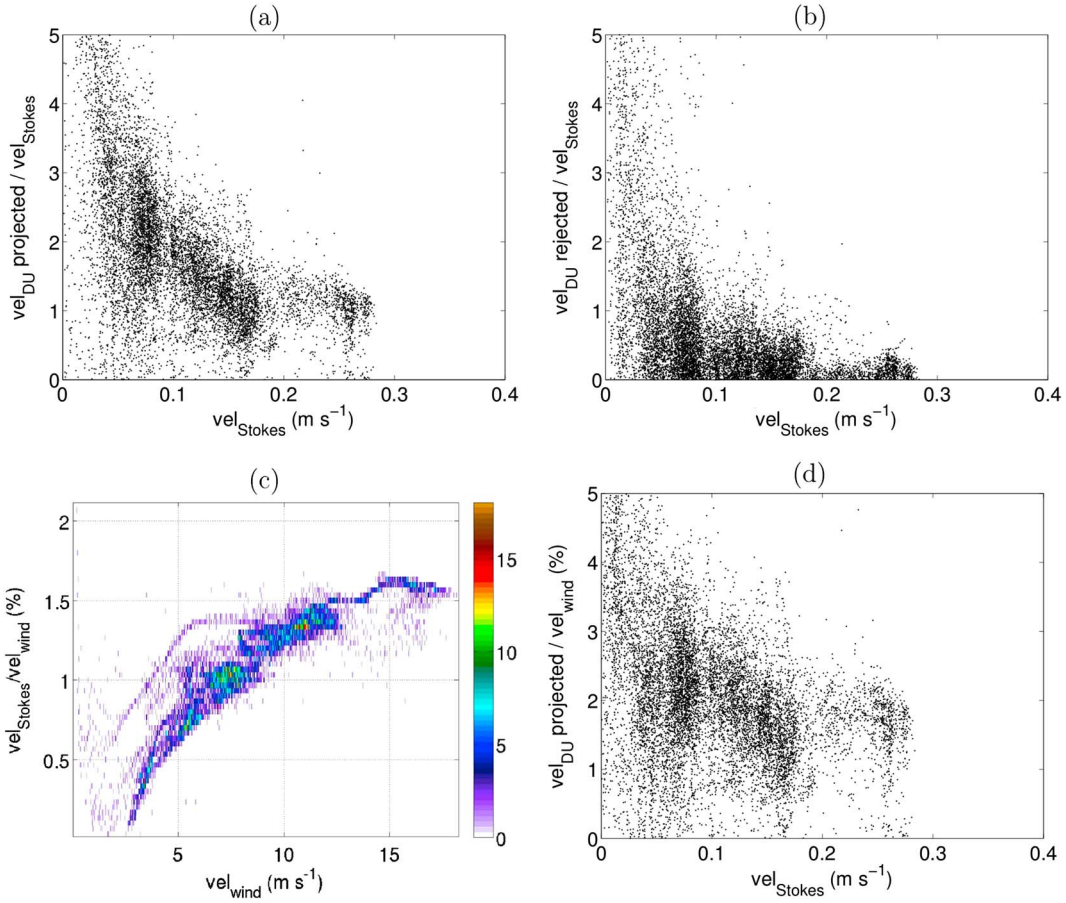

Figure 4. Projection (a) and rejection (b) of *DV* velocities on the Stokes drift, normalized. (c) Stokes drift relation to the 10-m winds at the overlapping locations (concentration scatterplot). (d) *DV* velocities compared to the 10-m wind speeds as a function of the Stokes drift.

(a) *DV versus Stokes drift* (Figure 4a): The projected component of *DV* on the Stokes drift has a value depending on the Stokes magnitude. For a significant drift (>10 cm/s), DV_{proj} is about 1–1.3 times the Stokes speed, while the rejected (normal to the Stokes drift, i.e., approximately crosswind) component DV_{rej} asymptotes to zero (Figure 4b). The downwind and crosswind components of *DV* for a large Stokes drift (>20 cm/s) seem therefore to indicate that during strong wind events, the velocity differential is mostly due to the action of the surface waves (as $vel_{\Delta V} \rightarrow vel_{Stokes}$). Note that during calm wind events, the underlying circulation becomes dominant, and thus the *DV* projection (and rejection) becomes meaningless in this context.

(b) *Stokes drift versus wind* (Figure 4c): Table 5 shows the dependence of the Stokes drift on the wind magnitude. One can see that at the overlapping locations, UWIN-CM produces a clear trend that is non-linear in terms of wind percentage: the Stokes drift ranges from 0.86% of the wind speed when it is low (5 cm/s) up to 1.65% wind speed at 25 cm/s magnitude (note that all these numbers are obtained from calculation of the median). Another important consideration is the fact that the wind and waves are almost always strongly correlated with one another, since waves are being mostly generated by strong wind events in winter, and swells are absent due to the enclosed geometry of the GoM. This trend was confirmed in Haza et al. (2018). For other regions directly connected to open oceans such as the Southern California in summer, for example, swells from the south and winds from the west would result in an additional crosswind component for the Stokes drift. Nevertheless in the GoM, the Stokes drift's contribution to transport can be substituted by a simple wind speed percentage in wind-based parameterizations.

(c) *DV versus wind* (Figure 4d): An estimate of *DV* based on the wind can be obtained by combining the above results. Table 5 shows that when the Stokes drift ≥10 cm/s (corresponding to winds ≥8 m/s), *DV* is on average ~1.6–1.7% of the wind speed. This implies that for moderate (or a certain magnitude range

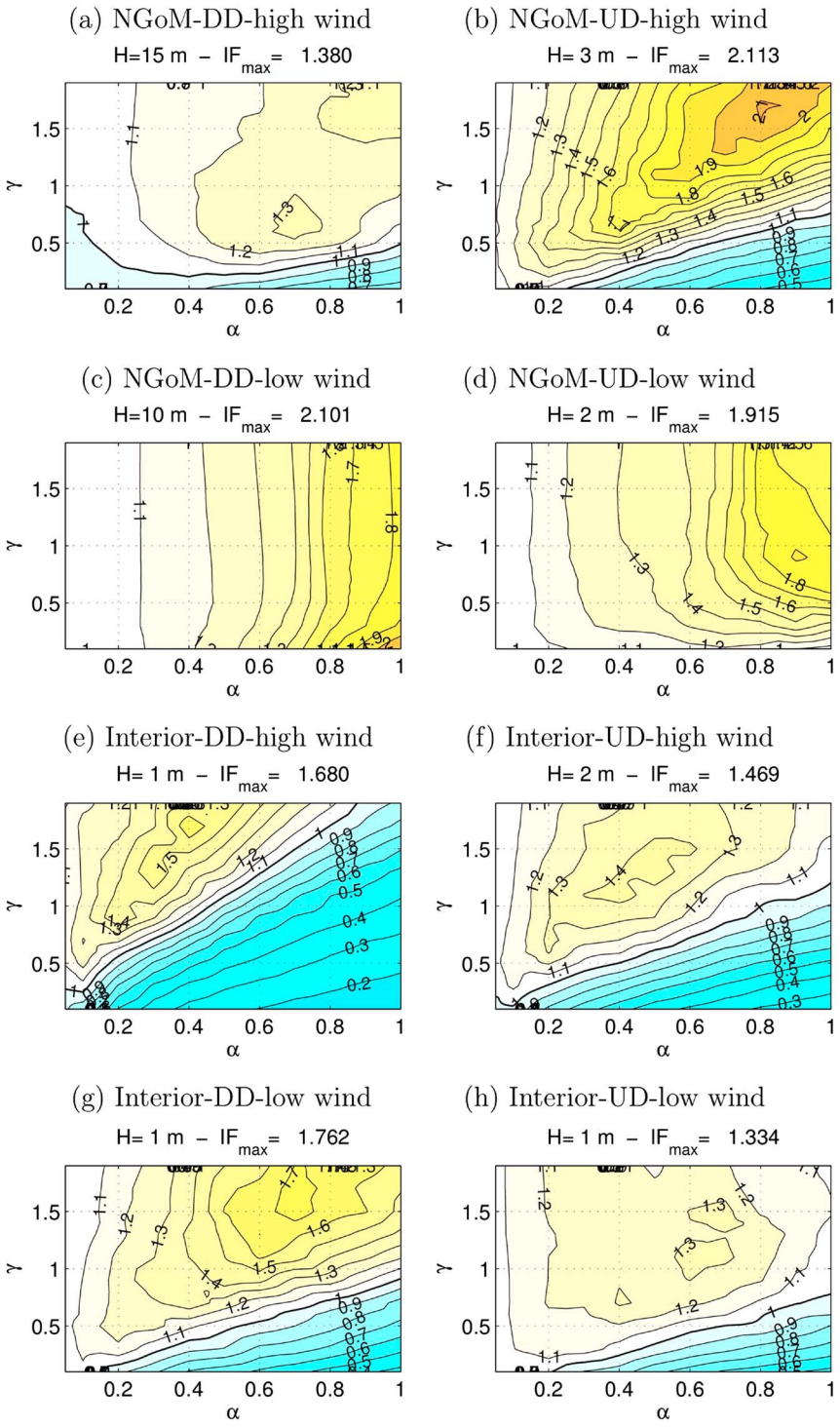

Figure 5. *H* selections improvement factor of the experimental matrix for the wind stress parameterization. (a–h) NGoM = northern Gulf of Mexico; DD = drogued drifters; UD = undrogued drifters.

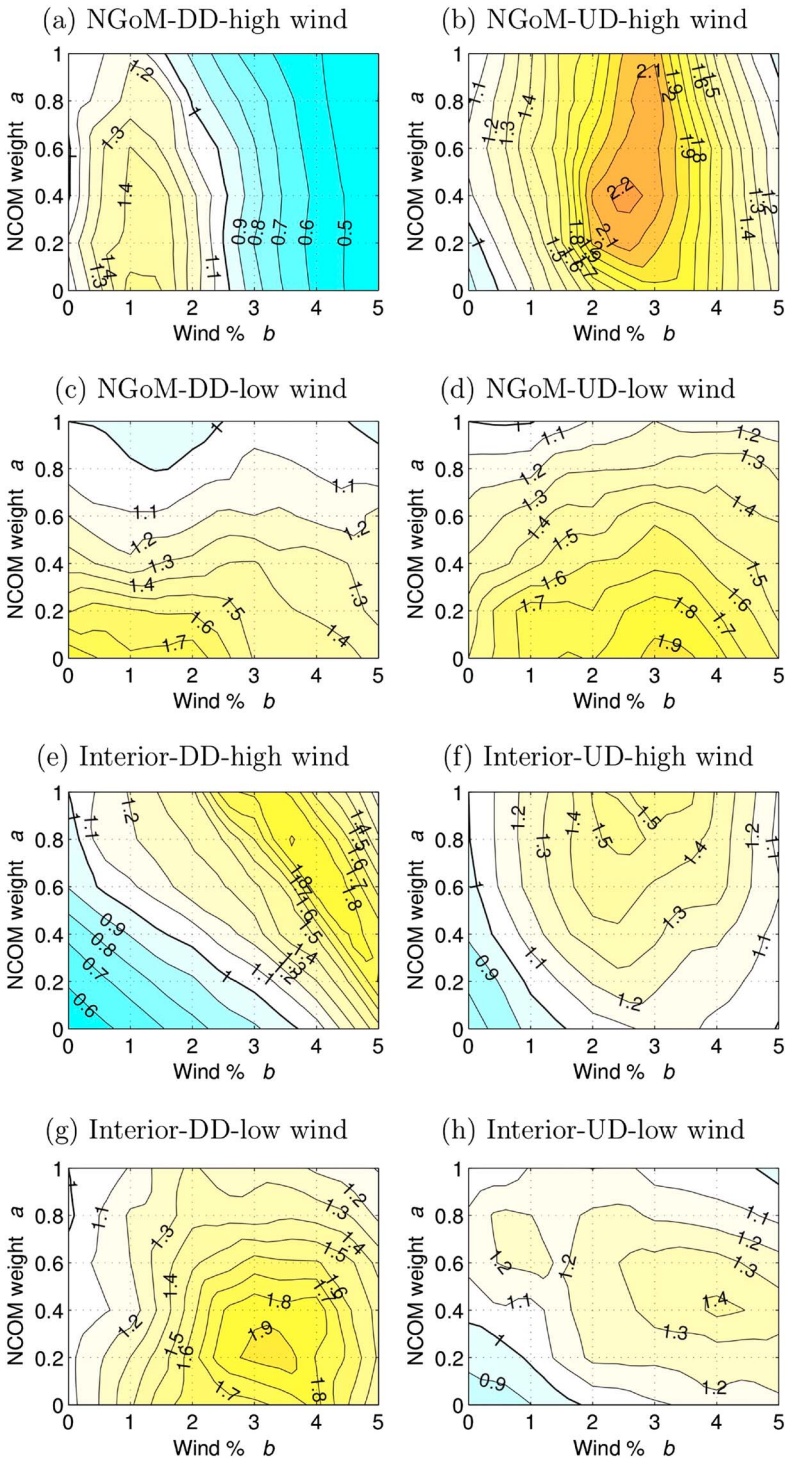

Figure 6. Improvement factor of the experimental matrix for the wind parameterization. (a–h) NGoM = northern Gulf of Mexico; DD = drogued drifters; UD = undrogued drifters.

of) winds, there is a wind component added to the Stokes drift in the upper 5 cm that is more substantial during lighter winds.

(d) *DV and laboratory experiments*: Assuming the remaining component must include the slip, a comparison to the laboratory experiments from Novelli et al. (2017) on the CARTHE drifters is warranted. It was found that the floater slip is significant, especially with the untethered floater. As the wind increases, so do the surface waves in amplitude and steepness, resulting in less exposure of the floater to the wind, which in turn reduces the slip. The slip is gradually reduced to zero as the waves reach a certain threshold. It appears then that there are two opposing factors leading to a quasi constant percentage of wind speed for *DV*: the Stokes drift increasing with the wind, and the floater slip decreasing with the wind. Compared to the free floater (UD), the slip of the DD is negligible. In laboratory experiments, Novelli et al. (2017) tested different U_{10} winds ranging from 8 to 23 m/s. The floater slip is about 1.7% U_{10} at 8-m/s speed, while it is only 0.37% for the DD, corresponding to a slip differential of 1.3% wind speed. Note that it is about twice the residual in *DV* during LASER for a similar wind speed, that is, 0.6% U_{10} after removing the Stokes component. Additionally, the full velocity differential in lab experiments is about 2.3% U_{10}, a value also substantially larger than the LASER *DV* at 1.7% U_{10}. For the strongest wind tested at 23 m/s in the lab, the slip differential becomes negligible and *DV* is reduced to 1.67% U_{10}, which corresponds to the asymptotic value of the Stokes drift in UWIN-CM. There is thus consistency between the laboratory results and the Stokes drift product of the coupled model for very strong winds. However, the non-Stokes component in LASER appears to be about half of what was observed in the laboratory experiments. This might be explained by considering the restricted conditions in the tank in terms of the realism of the waves, as well as the more extreme conditions at sea during LASER. Also, laboratory testing had occurred for half size drifters that were 3-D printed.

4.2. Representative Results From the Experimental Matrix

A wide range of parameters have been tested for both parameterizations. For reasons of brevity, we show only those cases that are most representative, or with the most pertinent impact. Note that in this section, the focus is on the sensitivity of *IF* to a variety of parameters in the experimental matrix, by using the statistical ensemble of trajectories described in the Methodology. In section 4.3, the emphasis will be on two individual events and how drifter trajectories are affected by the wind parameterizations.

Results are displayed in Figures 5 and 6, and summarized in Tables 6 and 7.

4.2.1. General Results

We first mention the averaged 2-day separation between ocean model and real LASER trajectories $\langle D(model)\rangle$, which ranges approximately between 19 and 29 km for the eight scenarios of the experimental matrix (see Table 6). Apart from the DD and UD scenarios at high winds in the NGoM, there are no obvious distinctions to be found. Even small errors in the flow field predictions from the mesoscale (in the GoM interior) and submesoscale (predominant in the NGoM) motions are sufficient to dominate the averaged separation and mask the impact of the wind-based component.

We find that the addition of the wind product substantially improves the model prediction by at least 30% and above 100%. (Note that a 100% improvement corresponds to an average reduction in the error for the ensemble 48-hr trajectories by a factor of 2). This is a significant improvement. The hybrid wind-stress parameterization was also tested with the COAMPS wind stress fields used intrinsically by NCOM, and nearly identical results as the UWIN-CM wind stress are found. There are two major implications. First, since the COAMPS fields are coarser (0.2° grid, ~27 km) than the 4-km UWIN-CM fields), the synoptic atmospheric features obviously play a major role in the wind contribution. And second, the prediction problem of NCOM is not due to its choice of wind product, but rather to its lack of contribution in the upper meter circulation that is part of the ocean surface layer (Anis & Moum, 1992).

Testing the sensitivity of the results to parameters $\delta = H/R$ and γ^* led to the following observations: Setting the Ekman depth, H, appears to have the same effect as redistributing a given kinetic energy quantity via the wind stress to a slab of thickness H. Decreasing H is therefore equivalent to increasing the slab velocity, and vice versa. On the other hand, γ^* was found to modify or alter the ocean velocity deviation from the wind expected from a steady state, with weak dependence on H. For instance, the deviation from the wind seems to be maximal at around 35–45° to the right for $\gamma^* \approx 0.5$ or below. Yet as γ^* increases, the deviation angle reduces down to about 12–15° to the right, corresponding to $\gamma^* \approx 1.9$. How much the Coriolis force deviates the wind-based downstream surface velocities can be in part explained by the relaxation time, which is

Table 6
Results of the Experimental Matrix for Both Wind-Stress ($V_{dr} = (1-\alpha)V_{mod} + \alpha V_{cor}$) and Wind ($V_{dr} = aV_{mod} + bV_{wind}$) Parameterizations

Parameterization		NGoM-DD-high winds	NGoM-UD-high winds
$\langle D(model)\rangle$		18.9 km	29.4 km
WStress	**IF**	**1.38**	**2.1**
	1-α, H	0–0.5; 6–20 m	0–0.5; 1–5 m
	γ	0.6–1.9	1.3–1.9
Wind	**IF**	**1.4–1.55**	**2.26**
	a	0–0.5	0.2–1, max at 0.4
	b	1–1.5%	2–3%
		NGoM-DD-low winds	NGoM-UD-low winds
$\langle D(model)\rangle$		26.2 km	19.2 km
WStress	**IF**	**2.1**	**1.9**
	1-α, H	0; 6–20 m	0.1; 1–6 m
	γ	weak dep, max at 0.1	0.5–1
Wind	**IF**	**1.8–1.9**	**1.93**
	a	0	0–0.1
	b	0-2%, max at 0-0.5%	3–3.5%
		Interior-DD-high winds	Interior-UD-high winds
$\langle D(model)\rangle$		27.5 km	28.1 km
WStress	**IF**	**1.5–1.7**	**1.45–1.5**
	1-α, H	0.5–0.7; 1 m	0.5–0.7; 1–2 m
	γ	1.3–1.9	1.3–1.9
Wind	**IF**	**1.92**	**1.55**
	a	0.8	0.9-1
	b	3.5%	2.5–3.5%
		Int-DD-low winds	Int-UD-low winds
$\langle D(model)\rangle$		23.8 km	23.0 km
WStress	**IF**	**1.6-1.8**	**1.33**
	1-α, H	0.2–0.4; 1 m	0.3–0.4; 1m
	γ	1.5–1.9	1–1.5
Wind	**IF**	**2.0**	**1.43**
	a	0.2–0.4	0.4
	b	3–3.5%	4–4.5%

Note. The 48-hr-averaged distance of the model-Lagrangian submesoscale experiment trajectories is also included. Parameters in green relate to the ocean model involvement, while parameters in red relate to wind-based momentum injection. NGoM = northern Gulf of Mexico; DD = drogued drifters; UD = undrogued drifters; IF = improvement factor. Bold font numbers refer to the IF values.

inversely proportional to γ^*. Very short relaxation times (~1 hr) correspond to high wind variability, which impede the Ekman balance for a steady state, while longer relaxation times allow for the Coriolis force to become important. γ^* is then a parameter controlling the deviation angle from the wind.

4.2.2. Results for the NGoM

This is a region devoid of any coherent structures associated with the mesoscales. We note that the wind contribution is easier to distinguish in the absence of mesoscales. For this reason we present the different scenarios on the NGoM extensively below. The results are interpreted by comparing the differing impacts of the oil thickness for a fixed wind strength (i.e., high or low sustained wind) and vice versa.

(a) *High winds: DD versus UD:* The wind-stress parameterization uses shorter depths for the UD than for the DD, that is, $1 \leq H \leq 2$ m versus $6 \leq H \leq 20$ m (Figures 5a and 5b). This translates into more wind-stress momentum injection for the UD. Similarly with the other parameterization, 2–3% of wind

Table 7
Results of the Experimental Matrix With Only the Wind Component ($\alpha = 1$)

Parameterization		NGoM-DD-high winds	NGoM-UD-high winds
WStress	**IF**	**1.38**	**2**
	H	15 m	4 m
	γ	1.9	1.5
	$\Delta\theta, \sigma$	−14.4° (6.3°)	−17.6° (11.7°)
Wind	**IF**	**1.55**	**1.9**
	b	1–1.5%	3–3.5%
		NGoM-DD-low winds	NGoM-UD-low winds
WStress	**IF**	**2.1**	**1.87**
	H	10 m	2 m
	γ	0.1, weak dep	0.9
	$\Delta\theta, \sigma$	−38° (55°)	−24.8° (18°)
Wind	**IF**	**1.8–1.9**	**1.93**
	b	0–2%, max at 0–0.5%	3–3.5%
		Interior-DD-high winds	Interior-UD-high winds
WStress	**IF**	**1.17**	**1.16**
	H	2 m	3 m
	γ	1.7	1.1–1.3
	$\Delta\theta, \sigma$	−13.7° (6.9°)	−16.2° (14.9°)
Wind	**IF**	**1.46**	**1.13**
	b	5%	3–3.5%
		Int-DD-low winds	Int-UD-low winds
WStress	**IF**	**1.66**	**1.11**
	H	2 m	1 m
	γ	1.1–1.3	1.5
	$\Delta\theta, \sigma$	−16.4° (10°)	−14.2° (8.6°)
Wind	**IF**	**1.8**	**1.18**
	b	4%	4–5%

Note. The median and standard deviation of the deviation angle from the wind ($\Delta\theta, \sigma$) is also computed for the wind stress parameterization. NGoM = northern Gulf of Mexico; DD = drogued drifters; UD = undrogued drifters; IF = improvement factor. Parameters in red relate to wind-based momentum injection. Bold font numbers refer to the IF values.

is injected for the UD versus only 1–1.5% for the DD (Figures 6a and 6b). In both cases, about half or less of the model velocities contribute to optimal improvement. The improvement factor is better for the UD ($IF > 2$) than for the DD ($IF \sim 1.5$). This makes sense, since the near-surface flow is more wind dependent. Note also a difference of 1–2% U_{10} between UD and DD, which is consistent with the estimated vertical shear from DD/UD overlaps of about 1.7% U_{10} for significant winds (Tables 5 and 4).

(b) *DD: high winds versus low winds:* Much higher improvement is seen for the low winds ($IF = 2.1$) than for the high winds ($IF = 1.5$), and by ignoring almost completely the ocean model (Figures 5a and 5c and 6a and 6c). Although it seems counterintuitive from the wind contribution, it does make sense from the perspective of the ocean model, because it confirms that in the absence of significant winds in the NGoM, the model cannot be properly constrained, since there are no mesoscales, and the LASER data set remains mostly at a distance from the river outflows, which is why relying solely on the wind can improve the prediction. Reversely, strong winds appear to constrain the model circulation, which explains the moderate IF with medium model involvement: The model is performing sufficiently well so that the wind or wind-stress injection can only improve so much. It is also worth noting that the submesoscales tend to be wiped out by strong winds and to reform in calm weather. When they do form, their main features should not be correlated with the ocean model which cannot constrain them at this present stage of development.

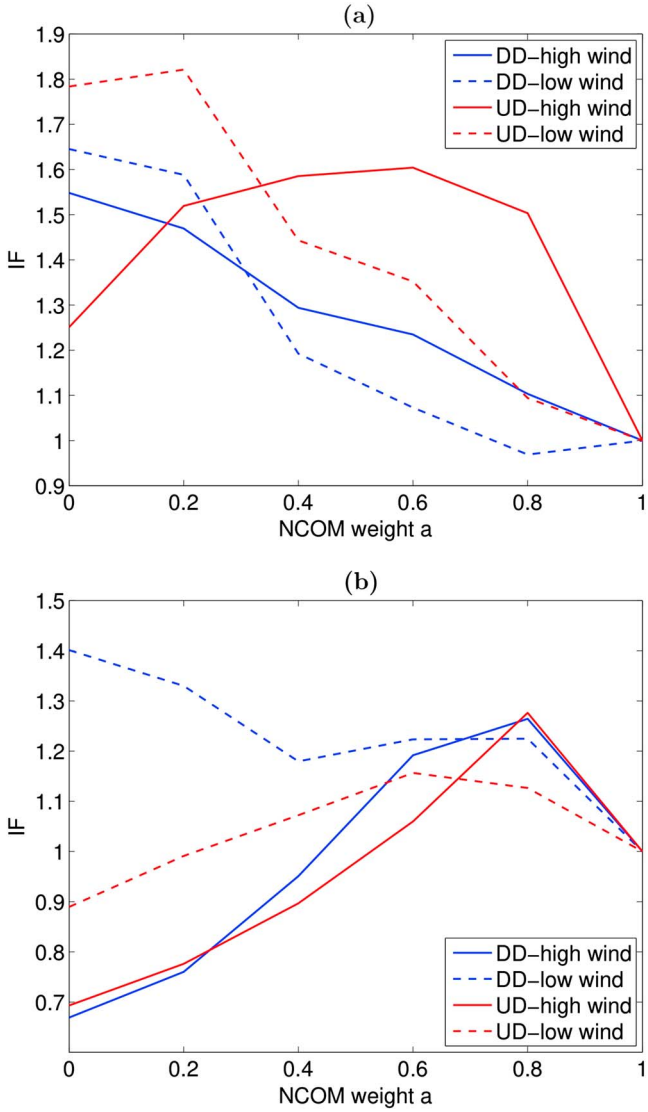

Figure 7. IF of the experimental matrix for the Stokes parameterization in (a) the NGoM and (b) the GoM interior, as a function of the NCOM model contribution. IF = improvement factor; NCOM = Navy Coordinate Ocean Model; DD = drogued drifters; UD = undrogued drifters.

(c) *Low winds: DD versus UD:* The improvement factor of both low wind cases is high around 2 and is obtained when suppressing the model velocities (Figures 5c and 5d and 6c and 6d). The main difference between DD and UD is in the injection of wind momentum, either via H or directly. In the latter case, 0–2% wind speed for DD versus 3–3.5% for UD yield optimum IF. That gap in wind percentage between DD and UD is wider than for the high wind cases, but it is likely due to the substantial floater slip during low winds. For instance, a relative slip of 1.3% U_{10} in the lab experiment was found for an 8-m/s wind (Table 4).

(d) *UD: high winds versus low winds:* There is even less model contribution involved for low winds. The higher wind percentage of 3–3.5% for low wind versus 2–3% for high wind (Figures 6b and 6d) accounts for the bigger slip as explained in (c). The IF is similar, ≈2.

4.2.3. Comparison of GoM Interior to NGoM

In the case of high winds and DD, and using the wind-stress parameterization, the predominant IF in the interior for $1 \leq H \leq 5$ m is 1.25–1.4 (Figure 5e). However, there is a small area in the parameter space of H=1 m where IF reaches 1.7. Overall, the optimal improvement requires in the interior smaller H of 1 to 2 m and a higher fraction of NCOM velocities between 0.7 and 0.9. On the other hand, the wind parameteriza-

Table 8
Ranges of Averaged Deviation Angles $\Delta\Theta$ Between the Wind Direction and the Corrected Lagrangian Velocities of the Wind-Stress Parameterization, for Different Values of the Parameter γ

γ	$\Delta\Theta$
0.5	[−45°, −35°]
0.9	[−31°, −23°]
1.5	[−14°, −20°]
1.9	[−16°, −12°]

Note. $\Delta\Theta$ values were calculated after removing the ocean model velocities.

tion gets better results with IF of 2 and an injection of 3.5% wind (Figure 6e). Generally, there is consistency between the two parameterizations. But in this case, the scenario of large a and b values (i.e., retaining most of the model AND injecting a big fraction of the wind) does not have its equivalent with the wind-stress injection, since both the ocean model (1-α) and τ (α) contributions cannot be large simultaneously. Comparing now with the wind parameterization, we see a model fraction of 0–0.5 versus 0.8, and a wind injection of 1–1.5% versus 3.5% for the NGoM and interior, respectively. Here, it is clear that the mesoscales are the reason for the higher reliance on NCOM. Yet it is less clear why the optimal H is reduced in the interior, that is why more kinetic energy input is needed from the wind/wind stress with respect to the NGoM. One possible explanation is that the altimetry product does not capture the entirety of the mesoscale field due to gaps in the spatiotemporal reconstruction of the geostrophic upper circulation. The excess wind-based Kinetic Energy (with respect to the NGoM) thus accounts for the downwind component of the existing mesoscale residual as well as submesoscale motions not captured by NCOM. It seems then that mesoscale circulation favors on average the downwind direction.

Regarding how GoM interior results compare with other cases, here are the main observations/trends. The mesoscale gradients also tend to mask the distinction between thick (DD) and thin (UD) drifter transports. The wind injection is in the range of about 3–4.5% U_{10} for all interior scenarios (Figures 6e–6h). During high wind events, more NCOM velocities are retained for optimal improvement than during low wind conditions, regarding both DD and UD trajectories. This trend was also present in the NGoM, albeit with a smaller fraction of the model velocities. In the interior, high winds require 0.8–1 of NCOM velocities (Figures 5e and 5f, and 6e and 6f) while low winds require 0.2–0.4 fraction (Figures 5g and 5h, and 6g and 6h). The difference in wind injection between UD and DD is not as high in the GoM interior (0–0.5% U_{10}) as in the NGoM (1–1.5% U_{10}), due also to mesoscale interference.

4.2.4. Stokes Drift Parameterization

With $\mathbf{V}_W = \mathbf{V}_{\mathrm{St}}$ in equation (5), only the surface Stokes drift is added to the NCOM velocities. The improvement factors of eight cases (DD vs. UD, high wind vs. low wind, NGoM vs. GoM interior) displayed in Figure 7 for different ocean model contributions indicate that if we replace the Stokes drift by a fraction of wind speed of ∼1% in low wind conditions and ∼1.5–2% in high wind conditions, similar IFs as found with the wind parameterization in Figure 6 can be obtained. In other words, the LASER data set confirms that the approximative relation observed in UWIN-CM outputs between the surface winds and Stokes drift is good enough to substitute the wave effect on surface transport by the 10 meter wind vectors. Note that this relation between surface wind and Stokes drift is valid only in the GoM at this particular time of the year, and shouldn't be generalized. The GoM is indeed shielded from remote mature swells, so that strong wind forcing waves are locally driven. In open basins however, the explicit Stokes drift should be considered.

4.2.5. Wind-Based Parameterizations Only

Here we take a closer look at the cases where the ocean model velocities are not included in the parameterization (i.e., $\alpha = 1$ and $a = 0$ for the Ekman and wind parameterizations, respectively). By isolating the effect of the wind from the ocean model component, we obtain from the best improvement factor the most likely contribution of the wind on the depth-integrated transport impacting the surface and near-surface flows. We also can extract the contribution of the Coriolis force on the wind stress in this regime of high wind variability. A comparison of Tables 6 and 7 indicates that for the NGoM, most of the optimal values do not change significantly when the ocean model velocities are removed. This means that in the NGoM, the wind is the major constraining factor for the near-surface circulation.

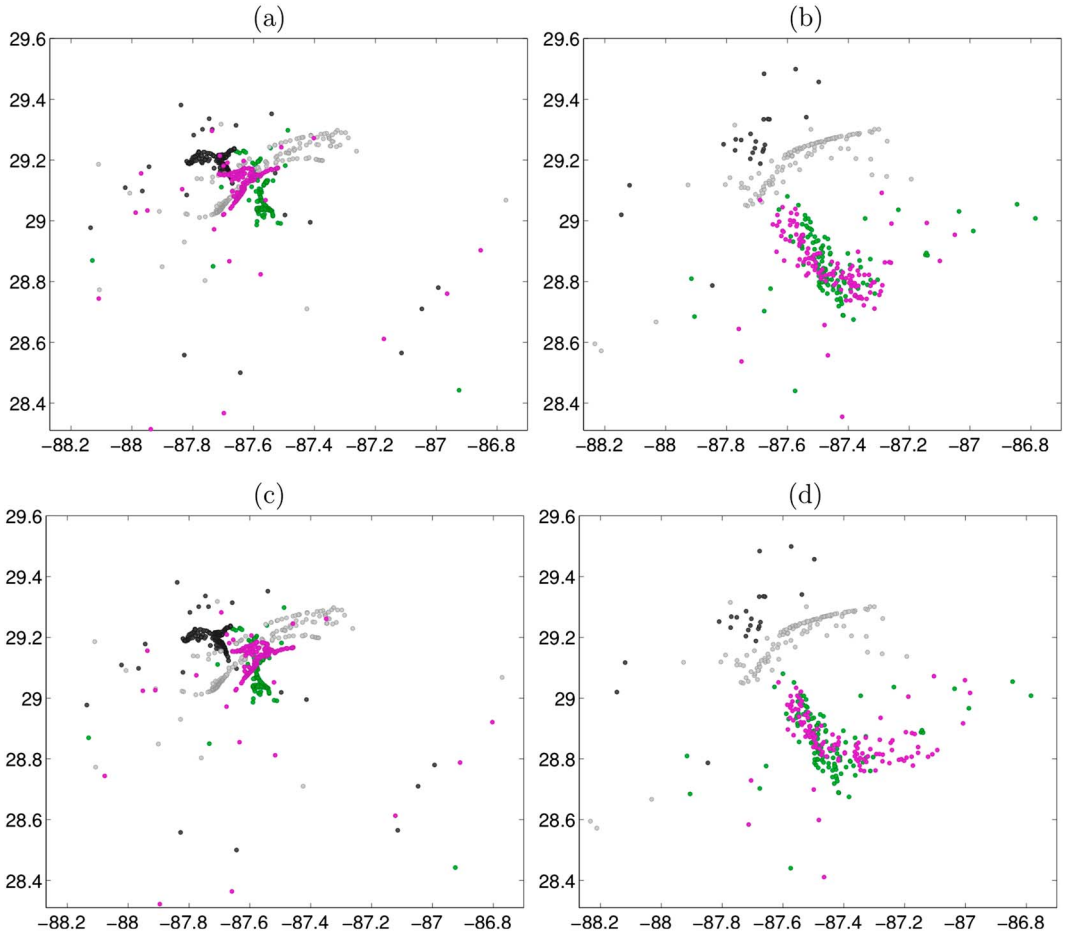

Figure 8. Testing the parameterizations during the Event 1 high wind period, centered on the Clover cluster. DD (a) and UD (b) initial positions are plotted in black. Their positions after about 2 days of Navy Coordinate Ocean Model advection is plotted in gray. The positions of the Lagrangian submesoscale experiment (a) DD and (b) UD at the same time are plotted in green, while the (optimally) parameterized positions via the Ekman model for the DD (a) and UD (b) are plotted in purple. (c and d) Same as (a) and (b) for the wind parameterization. DD = drogued drifters; UD = undrogued drifters.

In the upper 10–60 cm, 1–1.5% U_{10} is required at high winds, while about 0–0.5% only at low winds. In the upper 5 cm, however, the wind contribution is found to be independent of the wind magnitude, with an average of 3–3.5%. This constant addition at the surface accounts for three components more or less balancing out one another: the 10- to 60-cm wind contribution (U^w_{DD}), the Stokes drift (U^w_{Stokes}), and the floater slip (U^w_{slip}). Using estimates from the lab experiments (Table 4) and UWIN-CM, we have $U^w_{\mathrm{Stokes}} \sim 1.5\% \quad U_{10}$, U^w_{slip} ~0.5–0.8% U_{10} for high winds, while $U^w_{\mathrm{Stokes}} \sim 1\% \quad U_{10}$, $U^w_{\mathrm{slip}} \sim 1.7\% \quad U_{10}$ for low winds. Combined with U^w_{DD}, the wind contribution of the upper 5-cm averages around or above 3% wind speed.

We define $\Delta\theta$ as the deviation angle between the wind direction and the corrected Lagrangian velocities of the wind stress parameterization only . $\Delta\theta$ (Table 8) is linked to the Raleigh coefficient (due to Ekman transport) and tends to be smaller during high wind events (around 15°) than during low wind events (can be as large as 40°). The angle's normal distribution also has a smaller std associated with small $\Delta\theta$ .The high wind variability impedes the balance between friction and Coriolis force. The same effect applies to the Coriolis-Stokes forcing (Polton et al., 2005), since it takes more than a full inertial cycle to develop. As high wind speeds also lead to higher variability magnitudes, it might explain why the Coriolis deviation is more reduced during high winds.

In the GoM interior, removing NCOM velocities alters dramatically the IF of the wind stress parameterization for some cases. The improvement is reduced from the range of $1.33 \leq IF \leq 1.7$ down to $1.11 \leq IF \leq 1.17$. This is a confirmation that the mesoscale circulation captured by NCOM is crucial for

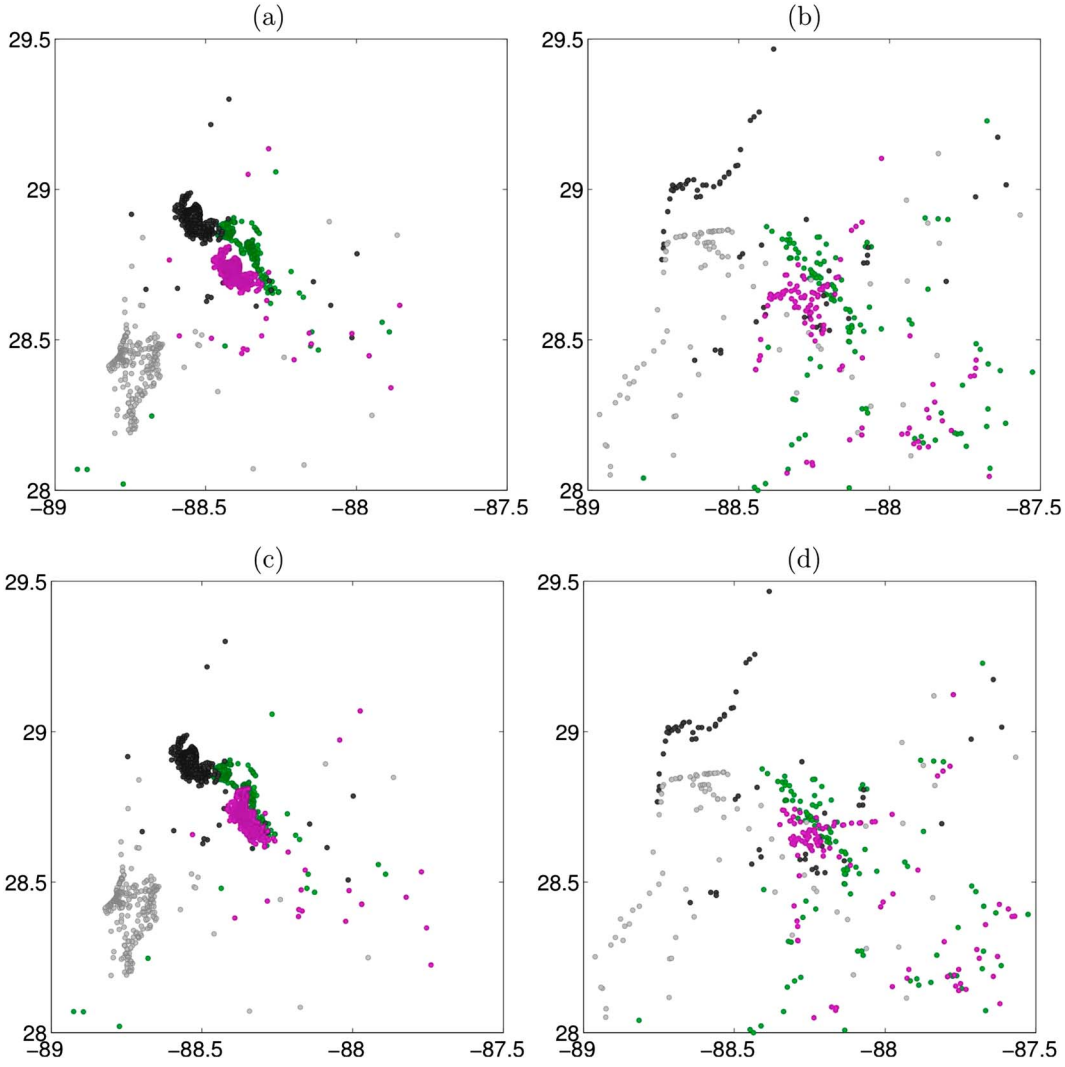

Figure 9. Same as Figure 8 for the Event 6 high wind period centered on the Last Drifter Array cluster.

a good improvement of Lagrangian prediction in the interior. As such, an additional 0.5–1% wind speed is required to account for the mesoscale downstream component, and it helps improve the performance by 10–20%. This is particularly true for the UD scenarios and for the wind-stress parameterization of the (DD, high) wind scenario. The exceptions to this trend are the (DD, low wind) cases, and the (DD, high wind) case with the wind parameterization.

4.2.6. Comparison to Relevant Past Studies

The comparison to Paldor et al. (2004) is done mainly about CARTHE drogued versus SVP drifters. Here again, significant differences arise, since we are attempting to fit the wind stress parameterization to the upper circulations of 0.6 and 0.05 m versus 15 m. The optimal IFs in this study tend to be obtained for higher values of γ and shorter mixing depths H, such as 6–20 m for the DD compared to the fixed 30-m depth for their analysis. They find an improvement of up to 43% in the tropical Pacific open ocean with the ECMWF winds, and by relying solely on the wind stress. In this study, aside from two cases where the optimal IFs are around 35%, we obtain improvements for the experimental matrix between 45% and 100%. Note that for individual events (i.e., specific drifter clusters such as P1 and/or LDA groups; see section 4.3), the improvement here is substantially higher. The drifter trajectories used in Paldor et al. (2004) also describe individual events. Additionally, more than half of the cases have relaxation times below 2 hr, compared to the 15–18 hr in Paldor et al. (2004). This is due in part to the higher output frequency of the UWIN-CM winds of 1 hr^{-1}, versus 1/6 hr^{-1} for the ECMWF product. We should be cautious in the conclusion, however, since

Table 9
(Addendum) Individual Event Results for the NGoM

Parameterization			NGoM-DD-high winds	NGoM-UD-high winds
Ev-1	WStress	**IF**	**1.7**	**4.9**
		1-α, H	0.5 ; 20 m	0.1–0.3 ; 4 m
	Wind	**IF**	**2.3**	**4.5**
		a	0.5	0.4–0.8
		b	0.5% (or 0–1%)	3%
Ev-3	WStress	**IF**	**1.6**	**3.3**
		1-α, H	0.3 ; low dep	0.1–0.3 ; 4 m
	Wind	**IF**	**1.7**	**3.8**
		a	0.4–0.5	0.2–0.3
		b	1%	1.5–2%
Ev-6	WStress	**IF**	**3**	**2.7**
		1-α, H	0–0.1 ; 5–10 m	0.1–0.3 ; 2–3 m
	Wind	**IF**	**3.3**	**4.6**
		a	0	0.2
		b	1–1.5%	3.5%
			NGoM-DD-low winds	NGoM-UD-low winds
Ev-2	WStress	**IF**	**2.1**	**2.8**
		1-α, H	0–0.1 ; 5–20 m, low dep	0–0.2 ; 1–3 m
	Wind	**IF**	**2**	**3.8**
		a	0	0
		b	0–2%, max at 1%	3–4%
Ev-4a	WStress	**IF**	**1.7**	**2.1**
		1-α, H	0.2 ; 6–10 m	0–0.2 ; 1–2 m
	Wind	**IF**	**1.6–1.7**	**2.5**
		a	0.2–0.4	0
		b	0–1%	2–3%
Ev-4b	WStress	**IF**	n/a	**2.3**
		1-α, H	n/a	0–0.2 ; 1–3 m
	Wind	**IF**	n/a	**2.3**
		a	n/a	0
		b	n/a	3%

Note. NGoM = northern Gulf of Mexico; IF = improvement factor; DD = drogued drifters; UD = undrogued drifters. Parameters in green and red relate to ocean model involvement and wind-based momentum injection, respectively. Bold font numbers refer to the IF values.

we are attempting to compare different regions (Pacific Ocean vs. GoM) and reference flows (drifter-based climatology vs. ocean forecast model).

Another relevant study is Le Hénaff et al. (2012), where wind-induced drift is combined with an oil circulation model under the same conditions as the DwH spill. The wind contribution in their case includes not only the Stokes drift but also the effect of wave breaking and Langmuir circulation. The combined effect amounts to about 2.4–2.9% wind speeds U_{10} (1.5–2% U_{10} for the Stokes drift, 0.9% U_{10} of Langmuir contribution) and a total deflection of about 20–25°. While the DwH spill occurred in the spring and into summer (LASER was in winter), it is worth noting that the UD cases for high and low wind in the NGoM are in the range of 2–3.5% U_{10}, which is very similar to the wind contribution of their model. The higher end is above their 2.4–2.9% estimate, but it includes also the floater slip particularly during light winds. The Langmuir contribution could account in part for the 1–1.5% U_{10} addition in the upper 10–60 cm, while the wave breaking component is most likely stronger during the bad weather conditions of LASER. Their wind deviation

Table 10
(Addendum) Individual Event Results for the GoM Interior

Parameterization			Interior-DD-high winds	Interior-UD-high winds
Ev-8a	WStress	**IF**	**1.5–1.8**	**1.5–1.8**
		1-α, H	0.2–0.5 ; 3–10 m	0.5–0.8 ; 1–5 m
	Wind	**IF**	**2.3**	**1.5**
		a	0.6–0.8	1
		b	1–2%	2–3%
			Interior-DD-low winds	Interior-UD-low winds
Ev-7a	WStress	**IF**	**1.4–1.8**	**1.25**
		1-α, H	0.2–0.3 ; 1m	0.6 ; 1m
	Wind	**IF**	**2.0**	**1.7**
		a	0.4–0.7	0.4–0.6
		b	3–4%	4%

Note. GoM = Gulf of Mexico; IF = improvement factor; DD = drogued drifters; UD = undrogued drifters. Parameters in green and red relate to ocean model involvement and wind-based momentum injection, respectively. Bold font numbers refer to the IF values.

is also similar to the average found in the NGoM without the model velocities if we combine the high and low wind scenarios.

While the surface wind-based parameterization of Stanichny et al. (2016) was implemented in the Black Sea using 15-m drogued SVP drifters, there are some interesting similarities to point out. The authors use also a simple formulation with two parameters regarding the wind fraction injected and the angle of deviation from the wind. At the very surface, they find that the wind-driven currents are deviated 13° to the right and with a magnitude of 2.8% wind velocity. We find in the NGoM for high winds at the surface a deviation of 17.5° with little variation, but 25° for lighter winds. Overall similar low deviation from the wind. A more dominant Stokes drift during high winds could explain the angle reduction. Optimal improvement without the ocean model in the NGoM in our study requires injection of 3–3.5% wind, which is higher than their estimate.

4.3. Individual Events

The results discussed are useful to quantify the influence of parameterizations on IF in a statistical sense, namely, the results are based on averages in space and time. Thus, they are not easy to visualize regarding their implication on drifter trajectories. In most practical applications, what is usually most important is whether trajectory prediction is improved during an "event," which would be associated with an oil spill, or other tracking problems, as outlined in the introduction. Next, we focus on how trajectory evolution is influenced during events. In particular, we take a closer look at two of those high wind events in the NGoM, since they illustrate really well the impact of NCOM on the IF and choice of parameters, as well as the role played by the wind product in improving the Lagrangian prediction: Event 1 is focused on the Clover (as part of P1) cluster, while Event 6 is centered on the LDA cluster.

(a) *Event 1.* Event 1 occurs shortly after the P1 launch on 22 January, following massive drogue losses, which resulted in the clover splitting into two groups. Very strong sustained winds provide here a good setting to observe how the parameterizations operate. In this case, the NCOM surface velocities do not differ much (at least in the first 24 hr) from the real flow as captured by the LASER DD (cf. Figure 8a): The advection from both on average looks like a southeast displacement. The NCOM field, however, produces later a circulation feature that is not realistic and constrains the particle cluster to spread and align along a modeled front (gray dots).
The optimum wind stress parameters for the DD case are [H=20 m, γ^*=1.7, and α=0.6] yielding IF = 1.67. In other words, a 70% improvement can be obtained by retaining 40% of the NCOM velocities and injecting wind stress KE in a 20-m-thick slab and Ekman deviation of ~16–20°. Indeed, the parameterized (purple) cluster after two days is closer to the LASER cluster than the NCOM group. For the UD group (Figure 8b), the optimal parameter set is [H=4 m, γ^*=1.5, and α=1] with an IF of 4.9. One

can see that reducing the slab thickness and ignoring the ocean model leads to a near identical bulk displacement as for the LASER UD drifters as illustrated by the green and purple dots.

Regarding the wind parameterization (Figures 8c and 8d), the best improvements are obtained for the DD case with $IF = 2.3$, [40% NCOM, 0.5% wind], and for the UD case with $IF = 4.5$, [40% NCOM, 3% wind].

Note that the results for both parameterizations are very similar, yet not identical. For instance, a better improvement is obtained for the DD case with the wind parameterization. It is interesting that their differences are minimal in spite of the Ekman deviation (with respect to the wind direction).

In both cases, the DD requires 40% NCOM velocities in combination with some wind-based momentum. This is due to the fact that the NCOM resolves part of the displacement due to the wind dominance affecting the underlying circulation as well during Event 1. The circulation features captured by the LASER drifters cannot be reproduced by the wind parameterizations if the ocean model does not. However, the advection from the wind contribution that is clearly underrepresented in the ocean model can be enhanced to reduce the gap between NCOM and observations.

Regarding UD, the wind contribution is expected to be much larger. In this case 3% wind is added for the UD group versus 0.5% for the DD group. The "thin-oil" surface prediction benefits from the wind parameterizations the most.

(b) *Event 6.* Event 6 (see parameterization tests illustrated in Figure 9) is an interesting case because the LDA cluster documents an important submesoscale features that is the confluence of strong density fronts. As expected, the ocean model gets it wrong and the NCOM advection dramatically diverges from reality. The improvement factor requires therefore little or no reliance on the ocean model. Figure 9a shows that the wind stress parameterization for the DD case with the optimal set [H=10 m, γ^*=1.3, and α=1] ignores the ocean model, which results in a translation of the LDA cluster, preserving its initial shape. While this translation is not representative of the real submesoscale feature, the overall displacement is adequate and a substantial correction from the NCOM-only advection. Hence, a high $IF = 3$ is attained. For the UD case (Figure 9b), a similar scenario is observed. Here again the wind-related translation is well captured by the Ekman parameterization using [H=3 m, γ^*=1.9, and α=1], while ignored in NCOM due in part to a spurious circulation feature, and in part because of the underrepresented vertical shear near the surface.

Here again, the difference between the DD and UD cases is in the momentum transfer, that is, for the wind stress parameterization, H is reduced from 10 to 3 m, while for the wind parameterization, 2% wind was added for the DD versus 3.5% for UD cases.

In general, for individual events, we find that the maximum improvement factors tend to be larger (cf. Tables 9 and 10). However, the IF dependence on the parameters of both parameterizations is quite similar to what is found for the experimental matrix. The only exception is for the DD-NGoM-High wind category. In those cases, the IF maps depend heavily on the performance of NCOM during that particular event.

5. Summary and Conclusions

Since the seminal work by Aref (1984), it is well understood that Lagrangian trajectories can be chaotic even in simple Eulerian flows that are different from one another in a minute way, in the presence of coherent structures (eddies of various scales, fronts by rivers, etc). These features set the Lagrangian pathways and small errors in their positions lead to exponential deviations in particle trajectories. While substantial progress has been made through satellite data assimilation to place mesoscale eddies in the right location in ocean models (Jacobs et al., 2014), submesoscales remain unconstrained. Our main thesis here is that, wind, unlike ocean features, has much larger scales, and due to the more advanced nature of atmospheric models via ubiquitous observations, atmospheric forecasts are quite accurate. For the near-surface ocean flows only, skillful use of wind therefore provides a reliable solution to reduce the challenge of chaotic advection that is chronically present in ocean models and is likely to remain so for the foreseeable future. The originality of this work is twofold. First, we study wind contribution in the presence of submesoscale motions that have been unresolved both observationally and numerically until recently. Second, we focus on two layers with unprecedented vicinity to the surface that have been inaccessible thus far.

As the dynamics of free surface and air-sea interface are not well captured by ocean models, the main objective is to assess and parameterize the impact of the wind for near-surface flows in a Lagrangian setting. The performance of two wind-based parameterizations (one based on the wind, the other based on the wind

stress) implemented with a Navy operational coastal ocean model in the GoM are assessed from the information provided by the LASER surface drifter data set. The UWIN-CM coupled atmosphere-wave-ocean model supplied the wind and wave fields at fine resolution, allowing to assess the contribution of skin drag, form drag and Stokes drift. The experimental matrix consisted of eight scenarios (Table 1) taking into account three types of distinction: oil thickness (thick/thin oil), location (NGoM/interior), and wind strength (high/low winds).

The main findings can be summarized as follows:

(a) The off-line addition of the wind product to the near-surface layer substantially improves the model prediction by 40–100% (note that 100% corresponds to reduction of the prediction error by a factor of 2). This results clearly indicates that modern ocean general circulation models can benefit from explicit incorporation of wind for surface transport problems. When combined to the knowledge that the COAMPS wind stress used intrinsically by NCOM can yield as good results as UWIN-CM with the hybrid parameterization, these results imply that the prediction problem of NCOM is not due to its choice of wind product (as long as the major fronts and features are correctly represented), but rather to its lack of dynamics in the upper meter circulation.

(b) *Performance under low wind conditions*. During low wind events in the NGoM, the optimal improvement requires relying only on the wind-product, since light winds are not strong enough to constrain the ocean model. Considering also the emergence of submesoscales during wind slackening episodes, which will inevitably diverge from their in situ counterparts. The improvement is as high as 100%.

(c) *Upper-ocean vertical shear*. In the NGoM, optimal improvements indicate also huge differences in terms of wind momentum injection between thick and thin oils, corresponding to about 1.5–2% wind speed, or much shorter mixing depths H for the upper 5-cm flow. For significant winds, that difference corresponds to the surface Stokes drift and the floater slip, which combined, make about 1.65–1.7% wind speed. Here the Stokes drift can be substituted by a wind percentage, since their directions are strongly correlated. Results can be as good without the ocean model. Note that the substitution of the Stokes drift by a fraction of the wind speed was made possible by the absence of remote swells in the GoM. In a domain more exposed to open ocean, the Stokes drift formulation would be more complex.

(d) *Upper-ocean wind contribution in the NGoM*. The wind contribution for both thick and thin oils varies depending on the strength of the wind, as inferred from best predictions of the wind-based parameterizations. In the upper 10–60 cm (thick oil), 1–1.5% wind speed is required at high winds, while 0–0.5% only at low winds. These numbers could account in part for the Langmuir contribution and wave breaking during high wind events, while submesocale motions tend to dominate the surface circulation during low wind events. Those results are consistent with other parameterizations (Le Hénaff et al., 2012). In the upper 5 cm, however, the wind contribution is found to be independent of the wind magnitude, with an average of 3–3.5%. This constant is due to the balance of three components: the 10- to 60-cm contribution, the Stokes drift, and the floater slip. While the Stokes drift increases with the wind, the slip decreases when the waves become more significant.

(e) *Contribution of wind parameterizations in mesoscale-rich GoM interior*. In the GoM interior, the ocean model plays more of a role. This is due to a large fraction of the mesoscale KE being reproduced by NCOM via assimilation of the altimetry product. However, the wind component added to optimize the parameterization has to be substantially higher than for the NGoM. This probably accounts for the downwind (or down Ekman) component of the existing mesoscale residual and submesoscale motions not captured by NCOM. There are however some reservations about the meaning of the wind-based parameterizations in the GoM interior, in that the addition of the wind component is no longer really targeting the ocean surface layer.

(f) *Deviation of the trajectories from the wind direction*. Implementing both parameterizations showed that the deviation is much less significant than what is predicted by the Ekman theory for a steady-state circulation and wind. For high winds in the NGoM, optimal improvements are obtained for wind deviations of $-18°$ to $-14°$, while that number can double during low winds with much more variability. It is clear that the high wind variability severely limits the balance between friction and Coriolis force. Similarly, the Coriolis-Stokes forcing (Polton et al., 2005), which takes at least a full inertial cycle to develop, must also be limited by the time-dependent winds. The important point here is that it explains why both parameterizations yield such similar results.

(g) *CARTHE versus SVP drifters.* By comparing CARTHE drifters with SVP drifters using results from Paldor et al. (2004), we find significant differences, since we are attempting to fit the hybrid wind-stress parameterization to upper circulations of 0.6 versus 15 m. Wind-stress momentum transfer depths H(DD) are shorter than H(SVP), accompanied by much shorter relaxation times. We also obtain higher improvement, although the comparison is limited, since we use different background flows and domains. Overall, it is not surprising to find that the upper 60- and 5-cm flows are more sensitive to the wind than the upper 15-m circulation.

Given what is presented in this study, one may wonder whether there is any reason to use a submesoscale resolving model. One can imagine (at least) three scenarios in which it is critical to operate submesoscale resolving models. The first is if a submesoscale process is absolutely critical to getting the transport pathways correctly. A good example of this is the disruption of the mesoscale transport barrier by submesoscales as well as how surface material is distributed by convergence zones. This problem was studied within the context of an eddy in the GoM by Haza et al. (2016). The second is presence of freshwater outflows that tend to control where pollutants propagating from offshore make landfall (Huguenard et al., 2016; Roth et al., 2017). In particular, near-field modeling of tidal outlets is where submesoscale resolving models can have great skill, because the transport problem is controlled by the tidal cycle as opposed to the phase of frontal instabilities. The third is the fact that submesoscale dynamics is a field that was discovered mostly through numerical modeling (McWilliams, 2016). Numerical models can create an environment in which researchers can experiment with and learn about submesoscale fluid dynamics, which then drives real ocean experiments for evaluation of model-based theories. A good example of this is the submesoscale experiment presented in Poje et al. (2014), the main parameters of which (number of drifters, release density, transmission frequency and duration) was designed on the basis of idealized submesoscale modeling by Özgökmen et al. (2012). These are some of the main reasons for running submesoscale resolving models. Ultimately, what is becoming clear is that high-resolution modeling must go hand in hand with high-resolution observations, not only to evaluate theories but also for data assimilation in forecasting.

Acknowledgments
This research was made possible by a grant from the Gulf of Mexico Research Initiative. Processed drifter trajectory data, drogue classification results, UWIN-CM, and NCOM model data are publicly available through the Gulf of Mexico Research Initiative Information and Data Cooperative (GRIIDC) at https://data.gulfresearchinitiative.org under DOIs 10.7266/N7W0940J, 10.7266/N7QN656H, 10.7266/N7KW5DH7, and 10.7266/N7HQ3WZR, respectively. The authors wish to thank the two anonymous reviewers who contributed to improving the manuscript.

References

Anis, A., & Moum, J. N. (1992). The superadiabatic surface layer of the ocean during convection. *Journal of Physical Oceanography*, *22*, 1221–1227.

Aref, H. (1984). Stirring by chaotic advection. *Journal of Fluid Mechanics*, *192*, 115–173.

Berta, M., Griffa, A., Magaldi, M. G., Özgökmen, T. M., Poje, A. C., Haza, A. C., & Olascoaga, M. J. (2015). Improved surface velocity and trajectory estimates in the Gulf of Mexico from blended satellite altimetry and drifter data. *Journal of Atmospheric and Oceanic Technology*, *32*(10), 1880–1901.

Chen, S. S., & Curcic, M. (2016). Ocean surface waves in Hurricane Ike (2008) and Superstorm Sandy (2012): Coupled modeling and observations. *Ocean Modelling*, *103*, 161–176. https://doi.org/10.1016/j.ocemod.2015.08.005

Chen, S. S., Zhao, W., Donelan, M. A., & Tolman, H. L. (2013). Directional wind-wave coupling in fully coupled atmosphere-wave-ocean models: Results from CBLAST-Hurricane. *Journal of the Atmospheric Sciences*, *70*, 3198–3215.

Curcic, M., Chen, S. S., & Özgökmen, T. M. (2016). Hurricane-induced ocean waves and Stokes drift and their impacts on surface transport and dispersion in the Gulf of Mexico. *Geophysical Research Letters*, *43*, 2773–2781. https://doi.org/10.1002/2015GL067619

D'Asaro, E. A., Shcherbina, A., Klymak, J. M, Molemaker, J., Novelli, G., Guigand, C. M., et al. (2018). Ocean convergence and the dispersion of flotsam. *Proceedings of the National Academy of Sciences*, *115*, 1162–1167. https://doi.org/10.1073/pnas.1718453115

Dietrich, J. C., Muhammad, A., Curcic, M., Fathi, A., Dawson, C. N., Chen, S. S., & Luettich Jr, R. A. (2018). Sensitivity of storm surge predictions to atmospheric forcing during Hurricane Isaac. *Journal of Waterway, Port, Coastal, and Ocean Engineering*, *144*(1), 04017035.

Donelan, M. A., Curcic, M., Chen, S. S., & Magnusson, A. K. (2012). Modeling waves and wind stress. *Journal of Geophysical Research*, *117*, C00J23. https://doi.org/10.1029/2011JC007787

Dvorkin, Y., Paldor, N., & Basdevant, C. (2001). Reconstructing balloon trajectories in the tropical stratosphere with a hybrid model using analyzed fields. *Quarterly Journal of the Royal Meteorological Society*, *127*(573A), 875–988.

Egbert, G. D., & Erofeeva, S. Y. (2002). Efficient inverse modeling of barotropic ocean tides. *Journal of Atmospheric and Oceanic Technology*, *19*, 183–204.

Haza, A. C., D'Asaro, E., Chang, H., Chen, S. S., Curcic, M., Guigand, C., et al. (2018). Drogue-loss detection of surface drifters during the Lagrangian submesoscale experiment (LASER). *Journal of Atmospheric and Oceanic Technology*, *35*, 705–725.

Haza, A. C., Özgökmen, T. M., & Hogan, P. (2016). Impact of submesoscales on surface material distribution in a Gulf of Mexico mesoscale eddy. *Ocean Modelling*, *107*, 28–48.

Hill, C., DeLuca, C., Balaji, V., Suarez, M., & da Silva, A. (2004). Architecture of the Earth System Modeling Framework. *Computing in Science and Engineering*, *6*, 18–28.

Hodur, R. M. (1997). The Naval Research Laboratory's Coupled Ocean/Atmosphere Mesoscale Prediction System (COAMPS). *Monthly Weather Review*, *125*(7), 1414–1430.

Huguenard, K. D., Bogucki, D. J., Ortiz-Suslow, D. G., Laxague, N. J. M., MacMahan, J. H., Özgökmen, T. M., et al. (2016). On the nature of the frontal zone of the Choctawhatchee Bay plume in the Gulf of Mexico. *Journal of Geophysical Research: Oceans*, *121*, 1322–1345. https://doi.org/10.1002/2015JC010988

Jacobs, G. A., Bartels, B. P., Bogucki, D. J., Beron-Vera, F. J., Chen, S. S., Coelho, E. F., et al. (2014). Data assimilation considerations for improved ocean predictability during the Gulf of Mexico Grand Lagrangian Deployment (GLAD). *Ocean Modelling*, *83*, 98–117.

Judt, F., Chen, S. S., & Curcic, M. (2016). Atmospheric forcing of the upper ocean transport in the Gulf of Mexico: From seasonal to diurnal scales. *Journal of Geophysical Research: Oceans*, *121*, 4416–4433. https://doi.org/10.1002/2015JC011555

Kenyon, K. E. (1969). Stokes drift for random gravity waves. *Journal of Geophysical Research*, *74*, 6991–6994.

Lagerloef, G. S. E., Mitchum, G. T., Lukas, R. B., & Niiler, P. P. (1999). Tropical Pacific near-surface currents estimated from altimeter, wind, and drifter data. *Journal of Geophysical Research*, *104*, 23,313–23,326.

Laxague, N. J. M., Özgökmen, T. M., Haus, B. K., Novelli, G., Shcherbina, A., Sutherland, P., et al. (2018). Observations of near-surface current shear help describe oceanic oil and plastic transport. *Geophysical Research Letters*, *45*, 245–249. https://doi.org/10.1002/2017GL075891

Le Hénaff, M., Kourafalou, V. H., Paris, C. B., Helgers, J., Aman, Z. M., Hogan, P. J., & Srinivasan, A. (2012). Surface evolution of the Deepwater Horizon oil spill patch: Combined effect of circulation and wind-induced drift. *Environmental Science & Technology*, *46*, 7267–7273.

McWilliams, J. (2016). Submesoscale currents in the ocean. *Proceedings of the Royal Society A*, *472*, 20160117.

Mensa, J. A., Garraffo, Z., Griffa, A., Özgökmen, T. M., Haza, A. C., & Veneziani, M. (2013). Seasonality of the submesoscale dynamics in the gulf stream region. *Ocean Dynamics*, *68*, 923–941.

Novelli, G., Guigand, C. M., Cousin, C., Ryan, E. H., Laxague, N. J. M., Dai, H., et al. (2017). A biodegradable surface drifter for ocean sampling on a massive scale. *Journal of Atmospheric and Oceanic Technology*, *34*, 2509–2532.

Olascoaga, M. J., Beron-Vera, F. J., Haller, G., Trinnanes, J., Iskandarani, M., Coelho, E. F., et al. (2013). Drifter motion in the Gulf of Mexico constrained by altimetric Lagrangian coherent structures. *Geophysical Research Letters*, *40*, 6171–6175. https://doi.org/10.1002/2013GL058624

Özgökmen, T. M., & Fischer, P. F. (2012). CFD application to oceanic mixed layer sampling with Lagrangian platforms. *International Journal of Computational Fluid Dynamics*, *26*, 337–348.

Özgökmen, T. M., Poje, A. C., Fischer, P. F., Childs, H., Krishnan, H., Garth, C., et al. (2012). On multi-scale dispersion under the influence of surface mixed layer instabilities and deep flows. *Ocean Modelling*, *56*, 16–30.

Paldor, N., Dvorkin, Y., & Basdevant, C. (2002). Improving the calculation of particle trajectories in the extratropical troposphere using standard NCEP fields. *Atmospheric Environment*, *36*, 483–490.

Paldor, N., Dvorkin, Y., Mariano, A. J., Özgökmen, T. M., & Ryan, E. H. (2004). A practical, hybrid model for predicting the trajectories of near-surface ocean drifters. *Journal of Atmospheric and Oceanic Technology*, *21*, 1246–1258.

Phillips, O. M. (1977). *Dynamics of the Upper Ocean*. Cambridge: Cambridge University Press.

Poje, A. C., Özgökmen, T. M., Lippjart, B., Haus, B., Ryan, E., Haza, A. C., et al. (2014). Submesoscale dispersion in the vicinity of the Deepwater Horizon spill. *Proceedings of the National Academy of Sciences*, *111*, 12,693–12,698. https://doi.org/10.1073/pnas.1402452111

Polton, J. A., Lewis, D. M., & Belcher, S. E. (2005). The role of wave-induced Coriolis-Stokes forcing on the wind-driven mixed layer. *Journal of Physical Oceanography*, *35*, 444–457.

Roth, M., MacMahan, J., Reniers, A., Özgökmen, T. M., Woodall, K., & Haus, B. (2017). Observations of inner shelf cross-shore surface material transport adjacent to a coastal inlet in the northern Gulf of Mexico. *Continental Shelf Research*, *137*, 142–153.

Skamarock, W. C., Klemp, J. B., Dudhia, J., Gill, D., Barker, D., Duda, M., et al. (2008). A description of the Advanced Research WRF version 3 (*NCAR/TN-475+STR*). Boulder, Colorado, USA: NCAR Technical Note.

Stanichny, S. V., Kubryakov, A. A., & Soloviev, D. M. (2016). Parameterization of surface wind-driven currents in the Black Sea using drifters, wind , and altimetry data. *Ocean Dynamics*, *66*, 1–10.

Stokes, G. G. (1847). On the theory of oscillatory waves. *Transactions of the Cambridge Philosophical Society*, *8*, 441.

Wallcraft, A. J., Metzger, E. J., & Carroll, S. N. (2009). Software design description for the HYbrid Coordinate Ocean Model (HYCOM) Version 904 2.2 (*NRL/MR/7320-09-9166*). Mississippi: Stennis Space Center.

Zhu, P., Wang, Y., Chen, S. S., Curcic, M., & Gao, C. (2016). Impact of storm-induced cooling of sea surface temperature on large turbulent eddies and vertical turbulent transport in the atmospheric boundary layer of Hurricane Isaac. *Journal of Geophysical Research: Oceans*, *121*, 861–876. https://doi.org/10.1002/2015JC011320